Exciton Superexchange, Resonance Pairs, and Complete Exciton Band Structure of $^1B_{2u}$ Naphthalene*

HWEI-KWAN HONG AND RAOUL KOPELMAN
Department of Chemistry, University of Michigan, Ann Arbor, Michigan 48104

(Received 17 August 1970)

A method for the determination of complete exciton band structures in molecular crystals is given. Pairwise exciton interactions are derived from resonance-pair data using an exciton "superexchange" approach. Koster and Slater's impurity cluster formulation is found to be applicable to nontrivial interchange symmetry systems, within the "restricted Frenkel–Davydov" theory. The derivation starts from the recent general formulation for isotopically mixed crystals of arbitrary concentrations. The resonance pair states are given by the second-order self-energy of the mixed crystal Green's function. General symmetry arguments and moment sum rules have been worked out for resonance pairs. It is demonstrated for naphthalene-h_8 resonance pairs in naphthalene-d_8 that superexchange corrections are not only inevitable for the $^1B_{2u}$ pair states but that they can also be utilized to assign experimental pairwise interactions to definite crystal directions, i.e., specific pairs. The naphthalene first singlet excited state 0–0 vibronic exciton band is successfully described by the "restricted Frenkel–Davydov" dispersion relation:

$$\epsilon(\mathbf{k}^{\pm}) = \sum_e M_e \exp(i\mathbf{k}\cdot\mathbf{R}_e) \pm \sum_i M_i \exp(i\mathbf{k}\cdot\mathbf{R}_i),$$

where $e=\mathbf{a}$, $\mathbf{b}$, $\mathbf{c}$, $(\mathbf{a}+\mathbf{c})$ and $i=\frac{1}{2}(\mathbf{a}+\mathbf{b})$, $[\frac{1}{2}(\mathbf{a}+\mathbf{b})+\mathbf{c}]$. Three sets of M's that are consistent with all resonance-pair and monomer mixed crystal data are tabulated. The only one consistent with a multipole expansion gives for the M_e's and M_i's, respectively, -0.6, -3.9, -3.7, 6.1, and 18.0, 2.0 cm^{-1}. This point multipole expansion is safely limited to nonnearest-neighbor interactions and truncated beyond transition octopoles ($Q_3^{1c}=7$ and $Q_3^{3c}=72$ Å^3). The translational shift is -4.5 ± 4 cm^{-1}, and the hot-band density-of-states function has been independently reproduced from the mixed crystal data, indicating that exciton–phonon coupling is small. The results are compared with *ab initio* calculations and new criteria for theoretical computations are suggested.

I. INTRODUCTION

We report here a determination of the complete exciton band in a molecular crystal, a method of assigning resonance pair data to specific pairwise interactions, and a confirmation of our recently derived density-of-states function.

The lowest excited states of molecular crystals are generally excitonic (tight-binding excitation) in nature. The Frenkel–Davydov theory[1] of these excitonic states depicts the energies of crystal eigenstates as a function of quasimomentum $\hbar\mathbf{k}$. Within this theoretical framework, the most important parameters are pairwise interactions. Most of the investigations in this field in the last decade have been involved with experimental determinations of related properties such as Davydov splittings, impurity states, band-to-band transitions, and exciton migration[2] while the direct attack on these parameters was limited to rough *ab initio* calculations.[3]

Recently, Hanson[4] investigated the fine structure around the "monomer" transition of some naphthalene-h_8 in d_8 mixed crystals, with concentrations ranging from a few thousandths of a percent to a few percent. He successfully identified some "resonance pair" ("dimer") absorption lines from their characteristic concentration dependence and polarization. Since the dimer splittings are, in the deep trap limit, determined solely by the interaction of the pair, Hanson obtained directly what may be termed "uncorrected" intermolecular interaction terms with both magnitude and sign.

Our recent experiments[5] on heavily doped mixed crystals of naphthalenes show that, at large energy gaps, cluster states similar to those reported by Hanson exist even at higher guest concentrations. As a matter of fact, the spectral features have been interpreted semiquantitatively in terms of Hanson's "isolated cluster states" at low concentrations plus a broadening due to the interactions among the "islands of guests." Therefore, the studies of these "isolated clusters" not only provide a possible means of elucidating intermolecular interactions but also form a basis toward a better understanding of more complex disordered systems.

In a recent paper, Hong and Robinson[6] (HR) presented a Green's function formulation for mixed crystals involving multiple-branched exciton bands as an extension of Yonezawa and Matsubara's[7] original work on electrons in a random lattice. The spirit of this formulation is different from that of the ordinary Koster and Slater[8] method in that it allows (in fact, it "requires," for statistical purposes) an arbitrarily large number of guests to be present as long as the concentration is held constant. A rigorous expression of the true propagator for mixed crystals of all concentrations was given as an infinite expansion in terms of the free propagator. In this paper, we will use the previous results as a starting point and examine the behavior of the mixed crystal Green's function at the dilute and infinitely dilute mixed crystal limit. It will be shown that the equations governing the energies of cluster (pair) states are formally the same as those of Koster and Slater's formalism.[8] However, the present

formulation has the advantage that all the possible cluster states are contained in a single expression, with proper weighing factors denoting the probability of finding these clusters. Moment expansions and sum rules are derived too. Symmetry rules for resonance pairs are given and discussed, with emphasis on the naphthalene-type crystal.

Actual calculations are performed on the energies of resonance pairs in the naphthalene–deuteronaphthalene systems. Since the deepest trap available by isotopic substitution is only 115 cm^{-1}, corresponding to naphthalene-h_8 in naphthalene-d_8 (compared with a bandwidth of 160 cm^{-1}) a large generalized quasiresonance effect was found (involving guest–host–guest interactions). The effect not only alters the magnitude of the splitting but also in some cases actually reverses the ordering of the levels predicted by a first-order argument.

The concept of exciton superexchange is introduced to further emphasize the above effect and a simple model is presented. A trial and error method has also been adopted to the study of resonance pairs of naphthalene-h_8 in naphthalene-d_8, using Hanson's data[4] and previous results of Davydov splittings and monomer quasiresonance[2f] as experimental checks. Because of the ambiguity involved in the assignments of the translationally equivalent pairs, several sets of interaction parameters were found. Attempts were also made to choose the best set consistent with the octopole model by Craig and Walmsley,[9] except for the explicit exclusion of nearest neighbors. It was found that one and only one set of interactions can be fitted, the unique octopole parameters being $Q_3^{1c}=7$ Å^3 and $Q_3^{3c}=72$ Å^3.

A comparison with previous *ab initio* calculations finds the latter still open to question. On the other hand, the recently determined experimental density-of-states function is found to be quite reliable, indicating that exciton–phonon coupling is of secondary importance in these systems. An empirical "site" approach to the pairwise interactions is discussed.

II. THEORY

A. Koster and Slater Equations and the Exciton Self-Energies

The energy eigenstates of one guest (monomer) and two guests (dimer) embedded in a host lattice were first treated by Koster and Slater.[8] The monomer

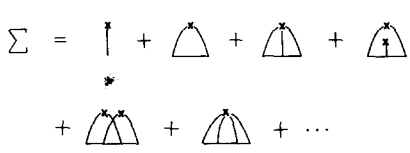

FIG. 1. Diagrams representing the expansion of the exciton self-energy in terms of the free propagator $G_0(\mathbf{k})$ [compare Eq. (4b)].

energy $E(1)$ and the dimer energies E_+, E_- can be obtained by solving the following determinants[10,6]:

for monomer:

$$1-\Delta\int[\rho_0(E')dE'/(E-E')]=0; \tag{1a}$$

for dimer:

$$\begin{vmatrix} 1-\Delta\int\frac{\rho_0(E')dE'}{(E-E')} & -\Delta\int\frac{\rho_R(E')dE'}{(E-E')} \\ -\Delta\int\frac{\rho_R(E')dE'}{(E-E')} & 1-\Delta\int\frac{\rho_0(E')dE'}{(E-E')} \end{vmatrix}=0, \tag{1b}$$

where Δ is the trap depth and $\rho_0(E')$ and $\rho_R(E')$ are the diagonal and off-diagonal density-of-states functions, respectively.[11] For example, for crystalline naphthalene in its $^1B_{2u}$ state, with two molecules per unit cell, it has been shown that,[6,10b] within the restricted Frenkel limit,[2b] ρ_0 and ρ_R can be written as

$$\rho_0(E')=N^{-1}\{\sum_{k^+}\delta[E'-\epsilon(\mathbf{k}^+)]+\sum_{k^-}\delta[E'-\epsilon(\mathbf{k}^-)]\}, \tag{2a}$$

and

$$\rho_R(E')=N^{-1}\{\sum_{k^+}\exp(i\mathbf{k}^+\cdot\mathbf{R})\delta[E'-\epsilon(\mathbf{k}^+)]\pm\sum_{k^-}\exp(i\mathbf{k}^-\cdot\mathbf{R})\delta[E'-\epsilon(\mathbf{k}^-)]\}, \tag{2b}$$

where $\epsilon(\mathbf{k}^+)$ and $\epsilon(\mathbf{k}^-)$ are the pure crystal exciton energies of the plus (A_u) and the minus (B_u) exciton branch, respectively.[12] N is the total number of molecules or states and $\mathbf{R}$ is the distance between the two molecules. The upper sign must be used for the translationally equivalent pair and the lower sign must be used for the interchange equivalent pair.[13] Equations (1) can be easily solved to yield the following expressions for $E(1)$ and E_+, E_-:

$$\int\{\rho_0(E')dE'/[E(1)-E']\}=1/\Delta, \tag{3a}$$

$$\int\{[\rho_0(E')\pm\rho_R(E')]dE'/(E_\pm-E')\}=1/\Delta. \tag{3b}$$

These are the familiar Koster and Slater relations.

In a more general approach, we may consider n guests, with n being large enough so that statistical averaging is a valid process (this is almost guaranteed, considering the actual number of guest molecules present even in a very dilute mixed crystal). It has been shown by HR that, within the restricted Frenkel limit, the mixed crystal Green's function can be written in Dyson's[14] form as[15a]

$$\langle G(\mathbf{k})\rangle=G_0(\mathbf{k})+G_0(\mathbf{k})\Sigma(\mathbf{k})\langle G(\mathbf{k})\rangle, \tag{4a}$$

and

$$\Sigma(\mathbf{k})=(\Delta/N)NP_1(c)+(\Delta/N)^2NP_2(c)\sum_{\mathbf{k}'}G_0(\mathbf{k}')$$
$$+(\Delta/N)^3[NP_3(c)\sum_{\mathbf{k}'}\sum_{\mathbf{k}''}G_0(\mathbf{k}')G_0(\mathbf{k}'')$$
$$+N^2P_1(c)P_2(c)\sum_{\mathbf{k}'}G_0(\mathbf{k}')G_0(\mathbf{k}')]$$
$$+(\Delta/N)^4N^2P_2^2(c)\sum_{\mathbf{k}_1}\sum_{\mathbf{k}_2}\sum_{\mathbf{k}_3}\bar{\delta}(\mathbf{k}-\mathbf{k}_1+\mathbf{k}_2-\mathbf{k}_3)$$
$$\times\bar{\delta}(\mathbf{k}_1-\mathbf{k}_2+\mathbf{k}_3-\mathbf{k})G_0(\mathbf{k}_1)G_0(\mathbf{k}_2)G_0(\mathbf{k}_3)$$
$$+(\Delta/N)^4NP_4(c)\sum_{\mathbf{k}'}\sum_{\mathbf{k}''}\sum_{\mathbf{k}'''}G_0(\mathbf{k}')G_0(\mathbf{k}'')G_0(\mathbf{k}''')+\cdots, \tag{4b}$$

where $c=n/N$ is the mole fraction of the impurity molecules and

$$G_0(\mathbf{k})=[E-\epsilon(\mathbf{k})]^{-1} \tag{4c}$$

is the pure crystal Green's function. Here $\langle G(\mathbf{k})\rangle$ is the mixed crystal Green's function. Any summation $\sum_{\mathbf{k}}$ includes all the $\mathbf{k}$ states in all the branches. $\Sigma(\mathbf{k})$ is the *exciton self-energy* and $P_\nu(c)$ is a polynomial given by the following generating function[16]:

$$\log(1-c+ce^x)=\sum_{\nu=1}^{\infty}\frac{P_\nu(c)x^\nu}{\nu!}. \tag{5}$$

The presence of $\bar{\delta}$, which will be defined below, is peculiar to the problem of multiple-branched exciton bands. As was stressed by HR, the "selection rules" for exciton scattering by impurities in multiple-branched exciton bands contain not only the conservation of quasimomentum (associated with translational symmetry) but also the retention of interchange symmetry[13b] (associated with factor group symmetry). Mathematically, we have[17]

$$\bar{\delta}(\mathbf{p}_1+\mathbf{p}_2+\mathbf{p}_3+\cdots+\mathbf{p}_s)$$
$$=\delta(\mathbf{p}_1+\mathbf{p}_2+\mathbf{p}_3+\cdots+\mathbf{p}_s)H[(-1)^m], \tag{6}$$

where $\mathbf{p}_1=\mathbf{k}-\mathbf{k}'$, $\mathbf{p}_2=\mathbf{k}'-\mathbf{k}''$, etc., are the momentum transfers between the impurities and the "exciton" in each encounter. $H[(-1)^m]$ is the Heaviside step function and m is the number of times an exciton is scattered from one branch of the band to the other; so

$$H[(-1)^m]=0, \quad \text{if} \quad m=\text{odd},$$
$$H[(-1)^m]=1, \quad \text{if} \quad m=\text{even}.$$

A diagrammatic method in which each expansion term is represented by a diagram in momentum space has been developed by Edwards[18] and by Klauder.[19] Equation (4b) can be depicted diagrammatically in Fig. 1.[15b] We have represented the free exciton propagator $G_0(\mathbf{k})$ by a horizontal line. Each vertex is associated with a polynomial $P_\nu(c)$, where ν equals the number of interaction lines connecting the impurity (represented by a cross) and the exciton propagator line. Each interaction line is associated with a momentum transfer $\mathbf{p}$ and since the net momentum transfer to a single impurity is zero, each vertex also carries a delta function [$\bar{\delta}$ in Eq. (6)]. The expansion can thus be written down easily by enumerating all the possible diagrams.

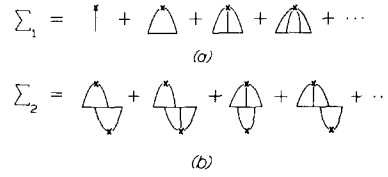

FIG. 2. (a) Diagrams included in the first-order self-energy part $\Sigma_1(\mathbf{k})$ which yields the single-impurity level. (b) Diagrams included in the second-order self-energy part $\Sigma_2(\mathbf{k})$ which yields the resonance pair levels.

The advantage of using the Green's function formalism is apparently its great versatility. First, the host and the guest are treated on equal footings so that the dual symmetry is retained.[20] Furthermore, it is a unified theory which is valid for the pure crystal on one extreme, for the dilute mixed crystal on the other (this is the problem treated in this paper), and for the heavily doped mixed crystals in between.[6] In the following, we will examine the behavior of the mixed crystal Green's function in the limit of infinite dilution. It will be demonstrated that in this limit the Green's function contains poles which correspond to the monomer state and also to the "isolated" pair (dimer) states.

1. *Monomers*

In order to locate the "isolated cluster states" including monomers, dimers, etc., we have to sum up diagrams involving one vertex, two vertices, etc., in Fig. 1. At low concentration of guests, the problem is simplified because the polynomial $P_\nu(c)\to 0$ for all ν when $c\to 0$. We limit our discussions to monomers and pairs and define Σ_1 and Σ_2 as shown diagrammatically in Fig. 2. Diagrams that are reducible such as the fourth one in Fig. 1 are of no concern here. Although the particular diagram has two vertices it actually represents the interactions between two different monomers. Physically such diagrams are responsible for the broadening of the monomer absorption line.

It is evident that when c approaches zero, the monomer partial sum is

$$\Sigma_1=(\Delta/N)Nc[1+\Delta G_0(E)+\Delta^2G_0^2(E)+\cdots]$$
$$=c\Delta/[1-\Delta G_0(E)], \tag{7a}$$

where

$$G_0(E)=1/N\sum_{\mathbf{k}'}G_0(\mathbf{k}')$$
$$=1/N[\sum_{\mathbf{k}^+}G_0(\mathbf{k}^+)+\sum_{\mathbf{k}^-}^{\mathbf{k}_0}G_0(\mathbf{k}^-)];$$

or, using Eqs. (2a) and (4c), we have

$$G_0(E)=\int[\rho_0(E')dE'/(E-E')]. \tag{7b}$$

Notice that Σ_1 has no $\mathbf{k}$ dependence. Furthermore, from Eqs. (4a) and (4c) we have

$$\langle G(\mathbf{k})\rangle = 1/[G_0(\mathbf{k})^{-1} - \Sigma(\mathbf{k})] = 1/[E - \epsilon(\mathbf{k}) - \Sigma(\mathbf{k})], \quad (8)$$

or taking the imaginary part of each side,

$$\mathrm{Im}\langle G(\mathbf{k})\rangle = \frac{\mathrm{Im}\Sigma(\mathbf{k})}{[E-\epsilon(\mathbf{k})-\mathrm{Re}\Sigma(\mathbf{k})]^2+[\mathrm{Im}\Sigma(\mathbf{k})]^2}. \quad (9)$$

Since at low concentration $\Sigma(\mathbf{k})$ is very small, we can put[21]

$$\mathrm{Im}\langle G(\mathbf{k})\rangle \simeq \mathrm{Im}\Sigma(\mathbf{k})/[E-\epsilon(\mathbf{k})]^2. \quad (10)$$

In other words, the poles of $\langle G(\mathbf{k})\rangle$ outside the band are the same as the poles of $\Sigma(\mathbf{k})$ and the residues of these two functions at their common poles are related through Eq. (10).

It follows immediately from Eqs. (7a) and (10) that the monomer energy, $E(1)$, must satisfy $(\Sigma \to \Sigma_1)$

$$1 - \Delta G_0(E) = 0$$

or

$$\int \{\rho_0(E')dE'/[E(1)-E']\} = 1/\Delta$$

which is the familiar Koster and Slater equation (3a).

The optical spectrum can also be obtained by using the following relationships[6]:

$$I_b^0(E) = \pi^{-1}\,\mathrm{Im}\langle G(\mathbf{k}^+=0)\rangle,$$

and

$$I_{ac}^0(E) = \pi^{-1}\,\mathrm{Im}\langle G(\mathbf{k}^-=0)\rangle. \quad (11a)$$

For convenience, we will work with $I_b(E(1))$ and $I_{ac}(E(1))$, defined as the total intensity attributable to the monomer impurity integrated over the neighborhood ϵ of $E(1)$:

$$I_b(E(1)) = \int_{E(1)-\epsilon}^{E(1)+\epsilon} I_b^0(E)dE,$$

$$I_{ac}(E(1)) = \int_{E(1)-\epsilon}^{E(1)+\epsilon} I_{ac}^0(E)dE. \quad (11b)$$

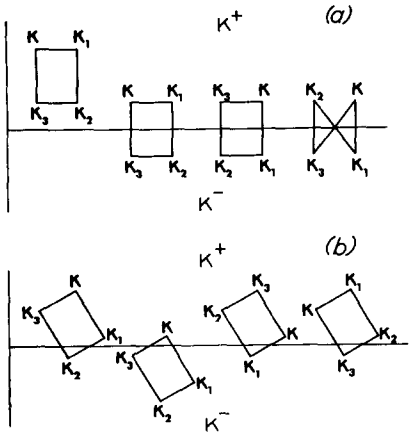

FIG. 3. Possible scattering routes given by $\bar{\delta}(\mathbf{k}-\mathbf{k}_1+\mathbf{k}_2-\mathbf{k}_3)\times\bar{\delta}(\mathbf{k}_1-\mathbf{k}_2+\mathbf{k}_3-\mathbf{k})$ according to our definition of the delta functions. Terms to be summed are those in (a) and terms *not* to be summed are those in (b).

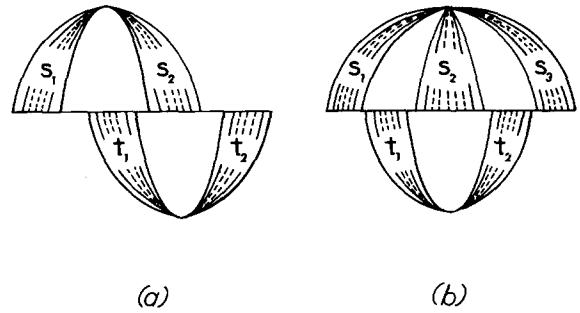

FIG. 4. (a) Typical diagrams included in $\Sigma_2(\mathbf{k})$. For convenience, diagrams of this type were summed up to form the partial sum that is represented by the first diagram in Fig. 5. (b) Typical diagrams included in $\Sigma_2(\mathbf{k})$. For convenience, diagrams of this type were summed up to form the partial sum that is represented by the second diagram in Fig. 5.

From Eqs. (10), (11a), and (11b), we found that

$$I_b(E(1)) = \pi^{-1}\int_{E(1)-\epsilon}^{E(1)+\epsilon} \frac{\mathrm{Im}\Sigma_1(\mathbf{k}^+=0)dE'}{[E'-\epsilon_b]^2} = \frac{\mathrm{res}\Sigma_1[E'=E(1)]}{[E(1)-\epsilon_b]^2}, \quad (12a)$$

where $\epsilon_b = \epsilon(\mathbf{k}^+=0)$. Since Σ_1 is $\mathbf{k}$ independent (and branch independent), $\Sigma_1(\mathbf{k}^+=0) = \Sigma_1(\mathbf{k}^-=0)$, we have similarly

$$I_{ac}(E(1)) = \frac{\mathrm{res}\Sigma_1(E'=E(1))}{[E(1)-\epsilon_{ac}]^2}, \quad (12b)$$

where $\epsilon_{ac} = \epsilon(\mathbf{k}^-=0)$. The polarization ratio $P(\mathbf{b}/\mathbf{ac})$, which is simply equal to $I_b \cdot |\mu_b|^2/I_{ac}\cdot|\mu_{ac}|^2$, can be rewritten as

$$P(\mathbf{b}/\mathbf{ac}) = [E(1)-\epsilon_{ac}]^2\cdot|\mu_b|^2/[E(1)-\epsilon_b]^2\cdot|\mu_{ac}|^2, \quad (12c)$$

where μ_b and μ_{ac} are the transition moments to the two Davydov components. This result has come to be known as the Rashba effect.[22]

Furthermore, the residue of Σ_1 at $E(1)$ can be evaluated from Eq. (7a) and substituted into Eq. (12). We find that

$$I_b(E(1)) = \{1/[E(1)-\epsilon_b]^2\}/[(d/dE)(\Sigma_1^{-1})]_{E=E(1)} = \frac{c}{[E(1)-\epsilon_b]^2}\left(\int\frac{\rho_0(E')dE'}{[E(1)-E']^2}\right)^{-1} = \{c\Delta^2/[E(1)-\epsilon_b]^2\}[dE(1)/d\Delta],$$

and

$$I_{ac}(E(1)) = \{c\Delta^2/[E(1)-\epsilon_{ac}]^2\}[dE(1)/d\Delta]. \quad (13)$$

These results were also derived by Craig and Philpott,[10a] based on the Koster and Slater formalism.

2. *Pairs*

Let us now turn to the pair problem. Σ_2 is $\mathbf{k}$ dependent and much more complicated to derive. The

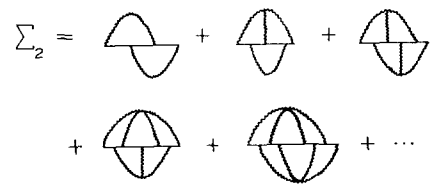

FIG. 5. Diagrams representing the expansion of $\Sigma_2(\mathbf{k})$ in terms of partial sums.

following procedure is an adaptation of Yonezawa and Matsubara's[7b] method to the multiple-branched exciton band. First, we examine the first diagram in Fig. 2(b) [or, equivalently, the fifth term in Eq. (4b)]. Our definition of the delta function $\bar{\delta}$ in Eq. (6) imposes certain restrictions with regard to the interchange symmetries of the states involved in the scattering. For this particular diagram, the implication of Eq. (6) is clear from Fig. 3. It is noted that only those scattering routes included in Fig. 3(a) are to be summed over although all the routes would be legitimate from a simple momentum consideration.

We define:

$$f_1(\mathbf{R})=\sum_{\mathbf{k}^+}\exp(i\mathbf{k}^+\cdot\mathbf{R})G_0(\mathbf{k}^+)+\sum_{\mathbf{k}^-}\exp(i\mathbf{k}^-\cdot\mathbf{R})G_0(\mathbf{k}^-),$$
$$f_2(\mathbf{R})=\sum_{\mathbf{k}^+}\exp(i\mathbf{k}^+\cdot\mathbf{R})G_0(\mathbf{k}^+)-\sum_{\mathbf{k}^-}\exp(i\mathbf{k}^-\cdot\mathbf{R})G_0(\mathbf{k}^-). \tag{14a}$$

Notice that, from Eq. (14a) and Eq. (2), we have

$$\begin{aligned} f_1(0)/N&=G_0(E)\\ &=\int[\rho_0(E')dE'/(E-E')],\\ f_1(\mathbf{R}_e)/N&=\int[\rho_{\mathbf{R}_e}(E')dE'/(E-E')],\\ f_2(\mathbf{R}_i)/N&=\int[\rho_{\mathbf{R}_i}(E')dE'/(E-E')], \end{aligned} \tag{14b}$$

where $\mathbf{R}_e$ is the pair distance between two translationally equivalent molecules and $\mathbf{R}_i$ is the pair distance between two interchange equivalent molecules.

The first diagram in Fig. 2(b) can be rewritten in terms of $f_1(\mathbf{R}_e)$ and $f_2(\mathbf{R}_i)$ [putting $P_r(c)=c$ for small c],

$$(\Delta/N)^4N^2c^2\sum_{\mathbf{k}_1}\sum_{\mathbf{k}_2}\sum_{\mathbf{k}_3}\bar{\delta}(\mathbf{k}-\mathbf{k}_1+\mathbf{k}_2-\mathbf{k}_3)\bar{\delta}(\mathbf{k}_1-\mathbf{k}_2+\mathbf{k}_3-\mathbf{k})G_0(\mathbf{k}_1)G_0(\mathbf{k}_2)G_0(\mathbf{k}_3)$$
$$=(\Delta/N)^4Nc^2[\sum_{\mathbf{R}_e}\exp(-i\mathbf{k}^{\pm}\cdot\mathbf{R}_e)f_1(\mathbf{R}_e)\mid f_1(\mathbf{R}_e)\mid^2\pm\sum_{\mathbf{R}_i}\exp(-i\mathbf{k}^{\pm}\cdot\mathbf{R}_i)f_2(\mathbf{R}_i)\mid f_2(\mathbf{R}_i)\mid^2]. \tag{15}$$

The upper sign should be used if the initial states are in the plus branch ($\mid\mathbf{k}^+\rangle$'s) and the lower sign should be used if they are in the minus branch ($\mid\mathbf{k}^-\rangle$'s). In deriving this, we have used the following equality:

$$\sum_{\mathbf{R}_e}\exp[-i(\mathbf{k}-\mathbf{k}_1+\mathbf{k}_2-\mathbf{k}_3)\cdot\mathbf{R}_e]+(-1)^m\sum_{\mathbf{R}_i}\exp[-i(\mathbf{k}-\mathbf{k}_1+\mathbf{k}_2-\mathbf{k}_3)\cdot\mathbf{R}_i]=N\bar{\delta}(\mathbf{k}-\mathbf{k}_1+\mathbf{k}_2-\mathbf{k}_3), \tag{16}$$

where $\bar{\delta}$ and m have been defined in Eq. (6).

Next we consider the third diagram in Fig. 2(b) (the second and fourth diagrams are actually variations of the same type, generalized from the first diagram, *vide infra*). This term can also be rewritten in terms of f_1 and f_2:

$$(\Delta/N)^5N^2c^2\sum_{\mathbf{k}_1}\sum_{\mathbf{k}_2}\sum_{\mathbf{k}_3}\sum_{\mathbf{k}_4}\bar{\delta}(\mathbf{k}-\mathbf{k}_1+\mathbf{k}_2-\mathbf{k}_3+\mathbf{k}_4-\mathbf{k})\bar{\delta}(\mathbf{k}_1-\mathbf{k}_2+\mathbf{k}_3-\mathbf{k}_4)G_0(\mathbf{k}_1)G_0(\mathbf{k}_2)G_0(\mathbf{k}_3)G_0(\mathbf{k}_4)$$
$$=(\Delta/N)^5Nc^2[\sum_{\mathbf{R}_e}\mid f_1(\mathbf{R}_e)\mid^4+\sum_{\mathbf{R}_i}\mid f_2(\mathbf{R}_i)\mid^4]. \tag{17}$$

In general, it is easy to see that terms represented by diagrams of the type in Fig. 4(a) [these would include, for example, the second and the fourth diagrams of Fig. 2(b)] can be written as

$$(\Delta/N)^4Nc^2[\sum_{\mathbf{R}_e}\exp(-i\mathbf{k}^{\pm}\cdot\mathbf{R}_e)f_1(\mathbf{R}_e)\mid f_1(\mathbf{R}_e)\mid^2$$
$$\pm\sum_{\mathbf{R}_i}\exp(-i\mathbf{k}^{\pm}\cdot\mathbf{R}_i)f_2(\mathbf{R}_i)\mid f_2(\mathbf{R}_i)\mid^2][(\Delta/N)f_1(0)]^{s-2}[(\Delta/N)f_1(0)]^{t-2}, \tag{18}$$

where $s=s_1+s_2$, $t=t_1+t_2$ [in reference to Fig. 4(a)] are the total numbers of interaction lines associated with each guest. Similarly, for diagrams of the type given in Fig. 4(b), we have

$$(\Delta/N)^5Nc^2[\sum_{\mathbf{R}_e}\mid f_1(\mathbf{R}_e)\mid^4+\sum_{\mathbf{R}_i}\mid f_2(\mathbf{R}_i)\mid^4][(\Delta/N)f_1(0)]^{s-3}[(\Delta/N)f_1(0)]^{t-2}, \tag{19}$$

where $s=s_1+s_2+s_3$ and $t=t_1+t_2$. These expressions can be derived from Eqs. (14) and (16).

It is apparent that diagrams with the same values of s and t but different values of s_1, s_2, s_3, t_1, t_2, etc., are actually equal and can be lumped together. The problem is, then, to calculate the number of possible partitions of s or t interaction lines into two or three groups. This general problem was treated by Yonezawa and Matsubara.[7b] We will use their results here. If we denote the number of all possible partitions of s interaction lines into r groups as $B_{s,r}$, we have

$$B_{s,r}=(s-1)!/(s-r)!(r-1)!, \tag{20}$$

or, alternatively, $B_{s,r}$ can be given by a generating function:

$$\left(\frac{x}{1-x}\right)^r = \sum_{s=r}^{\infty} B_{s,r} x^s. \tag{21}$$

Infinite sums over all diagrams of the type represented in Fig. 4(a) or 4(b) can now be performed with the aid of Eqs. (20) and (21). Denoting these sums as $S_{2,2}$ or $S_{3,2}$ (subscripts referring to the number of groups of interaction lines associated with the 1st and the 2nd guest, respectively), we have, from Eq. (18),

$$\begin{aligned} S_{2,2} &= (\Delta/N)^4 Nc^2 \Big[\sum_{\mathbf{R}_e} \exp(-i\mathbf{k}^{\pm}\cdot\mathbf{R}_e) f_1(\mathbf{R}_e) \mid f_1(\mathbf{R}_e) \mid^2 \pm \sum_{\mathbf{R}_i} \exp(-i\mathbf{k}^{\pm}\cdot\mathbf{R}_i) f_2(\mathbf{R}_i) \mid f_2(\mathbf{R}_i) \mid^2\Big] \\ &\quad \times \Big\{\sum_{s=2}^{\infty} B_{s,2}\big[(\Delta/N) f_1(0)\big]^{s-2}\Big\}\Big\{\sum_{t=2}^{\infty} B_{t,2}\big[(\Delta/N) f_1(0)\big]^{t-2}\Big\} \\ &= Nc^2 \Big[\sum_{\mathbf{R}_e} \exp(-i\mathbf{k}^{\pm}\cdot\mathbf{R}_e) f_1(\mathbf{R}_e) \mid f_1(\mathbf{R}_e) \mid^2 \pm \sum_{\mathbf{R}_i} \exp(-i\mathbf{k}^{\pm}\cdot\mathbf{R}_i) f_2(\mathbf{R}_i) \mid f_2(\mathbf{R}_i) \mid^2\Big] \\ &\quad \times \big\{(\Delta/N)/\big[1-(\Delta/N) f_1(0)\big]\big\}^4. \end{aligned} \tag{22a}$$

Similarly, from Eq. (19),

$$\begin{aligned} S_{3,2} &= (\Delta/N)^5 Nc^2 \Big[\sum_{\mathbf{R}_e} \mid f_1(\mathbf{R}_e) \mid^4 + \sum_{\mathbf{R}_i} \mid f_2(\mathbf{R}_i) \mid^4\Big]\Big\{\sum_{s=3}^{\infty} B_{s,3}\big[(\Delta/N) f_1(0)\big]^{s-3}\Big\}\Big\{\sum_{t=2}^{\infty} B_{t,2}\big[(\Delta/N) f_1(0)\big]^{t-2}\Big\} \\ &= Nc^2 \Big[\sum_{\mathbf{R}_e} \mid f_1(\mathbf{R}_e) \mid^4 + \sum_{\mathbf{R}_i} \mid f_2(\mathbf{R}_i) \mid^4\Big]\big\{(\Delta/N)/\big[1-(\Delta/N) f_1(0)\big]\big\}^5. \end{aligned} \tag{22b}$$

These two partial sums are represented by the first two diagrams in Fig. 5 where the second-order self-energy, Σ_2, is written as a *sum* of these *partial sums* (each one of them, in turn, is an infinite *sum*).

From the above discussion, a generalization can now be made concerning other partial sums in Fig. 5. In general, the odd-numbered partial sums [i.e., the $(2r-3)$th diagrams in Fig. 5, for $r \geq 2$] contain terms of the type:

$$\begin{aligned} &(\Delta/N)^{2r} Nc^2 \Big[\sum_{\mathbf{R}_e} \exp(-i\mathbf{k}^{\pm}\cdot\mathbf{R}_e) f_1(\mathbf{R}_e) \mid f_1(\mathbf{R}_e) \mid^{2(r-1)} \\ &\qquad \pm \sum_{\mathbf{R}_i} \exp(-i\mathbf{k}^{\pm}\cdot\mathbf{R}_i) f_2(\mathbf{R}_i) \mid f_2(\mathbf{R}_i) \mid^{2(r-1)}\Big]\big[(\Delta/N) f_1(0)\big]^{s-r}\big[(\Delta/N) f_1(0)\big]^{t-r}, \end{aligned} \tag{23a}$$

which are summed to give

$$\begin{aligned} S_{r,r} &= Nc^2 \Big[\sum_{\mathbf{R}_e} \exp(-i\mathbf{k}^{\pm}\cdot\mathbf{R}_e) f_1(\mathbf{R}_e) \mid f_1(\mathbf{R}_e) \mid^{2(r-1)} \\ &\qquad \pm \sum_{\mathbf{R}_i} \exp(-i\mathbf{k}^{\pm}\cdot\mathbf{R}_i) f_2(\mathbf{R}_i) \mid f_2(\mathbf{R}_i) \mid^{2(r-1)}\Big]\left(\frac{\Delta/N}{1-(\Delta/N) f_1(0)}\right)^{2r}. \end{aligned} \tag{23b}$$

Similarly, the even-numbered partial sums [corresponding to the $(2r-2)$th diagram in Fig. 5] contain terms of the type:

$$(\Delta/N)^{2r+1} Nc^2 \Big[\sum_{\mathbf{R}_e} \mid f_1(\mathbf{R}_e) \mid^{2r} + \sum_{\mathbf{R}_i} \mid f_2(\mathbf{R}_i) \mid^{2r}\Big]\big[(\Delta/N) f_1(0)\big]^{s-r-1}\big[(\Delta/N) f_1(0)\big]^{t-r}, \tag{24a}$$

which are summed, again, to give

$$S_{r+1,r} = Nc^2 \Big[\sum_{\mathbf{R}_e} \mid f_1(\mathbf{R}_e) \mid^{2r} + \sum_{\mathbf{R}_i} \mid f_2(\mathbf{R}_i) \mid^{2r}\Big]\left(\frac{\Delta/N}{1-(\Delta/N) f_1(0)}\right)^{2r+1}. \tag{24b}$$

We are now in a position to perform the summation in Fig. 5. So, finally, we have

$$\begin{aligned} \Sigma_2(\mathbf{k}^{\pm}) &= \sum_{r=2}^{\infty} (S_{r,r} + S_{r+1,r}) = \frac{(\Delta/N)^4 Nc^2}{\big[1-(\Delta/N) f_1(0)\big]^3} \\ &\quad \times \left(\sum_{\mathbf{R}_e} \frac{\exp(-i\mathbf{k}^{\pm}\cdot\mathbf{R}_e) f_1(\mathbf{R}_e) \mid f_1(\mathbf{R}_e) \mid^2 \big[1-(\Delta/N) f_1(0)\big] + (\Delta/N) \mid f_1(\mathbf{R}_e) \mid^4}{\big[1-(\Delta/N) f_1(0)\big]^2 - \mid (\Delta/N) f_1(\mathbf{R}_e) \mid^2}\right. \\ &\quad \left. + \sum_{\mathbf{R}_i} \frac{\pm \exp(-i\mathbf{k}^{\pm}\cdot\mathbf{R}_i) f_2(\mathbf{R}_i) \mid f_2(\mathbf{R}_i) \mid^2 \big[1-(\Delta/N) f_1(0)\big] + (\Delta/N) \mid f_2(\mathbf{R}_i) \mid^4}{\big[1-(\Delta/N) f_1(0)\big]^2 - \mid (\Delta/N) f_2(R_i) \mid^2}\right). \end{aligned} \tag{25}$$

It can be seen that for general $\mathbf{k}^+$ and $\mathbf{k}^-$, the second-order self-energy contains poles which correspond to the energy states of resonance pairs with varying separations ($\mathbf{R}_e$ and $\mathbf{R}_i$). Furthermore, these pairs are equally

probable (c^2 dependence). At the poles, the following equations are satisfied: For translationally equivalent pairs,

$$[1-(\Delta/N)f_1(0)]^2-\mid(\Delta/N)f_1(\mathbf{R}_e)\mid^2=0, \tag{26a}$$

and for interchange equivalent pairs,

$$[1-(\Delta/N)f_1(0)]^2-\mid(\Delta/N)f_2(\mathbf{R}_i)\mid^2=0. \tag{26b}$$

As we noted earlier,[11] $f_1(\mathbf{R}_e)$ and $f_2(\mathbf{R}_i)$ are usually real. The solutions to Eqs. (26a) and (26b) are then

$$f_1(0)/N\pm f_1(\mathbf{R}_e)/N=1/\Delta \tag{27a}$$

and

$$f_1(0)/N\pm f_2(\mathbf{R}_i)/N=1/\Delta. \tag{27b}$$

The equivalence between Eqs. (27a), (27b), and Eq. (3b) can be easily established through Eq. (14b).

As for the optical spectrum, we simply put $\mathbf{k}^{\pm}=0$. Thus for *translationally equivalent pairs*, we have from Eq. (25)

$$\Sigma_2(\mathbf{k}^+=0)=\Sigma_2(\mathbf{k}^-=0)=\frac{(\Delta/N)^4Nc^2f_1(\mathbf{R}_e)\mid f_1(\mathbf{R}_e)\mid^2}{[1-(\Delta/N)f_1(0)]^3\{[1-(\Delta/N)f_1(0)]-[(\Delta/N)f_1(\mathbf{R}_e)]\}}, \tag{28a}$$

so that only one state E_+ is optically allowed. Again, f_1 is real and *at the pole*, we have

$$\Sigma_2(\mathbf{k}^+=0)=\Sigma_2(\mathbf{k}^-=0)=\frac{\Delta c^2}{[1-(\Delta/N)f_1(0)]-[(\Delta/N)f_1(\mathbf{R}_e)]}. \tag{28b}$$

The spectral functions I_b and I_{ac} which have been discussed before in connection with the optical properties of the monomer can also be found through Eqs. (12a) and (28). We have

$$\begin{aligned} I_b(E_+)&=\frac{1}{[E_+-\epsilon_b]^2}\left[\frac{d}{dE}\left(\frac{1}{\Sigma_2}\right)\right]^{-1}_{E=E+}\\ &=\frac{c^2}{[E_+-\epsilon_b]^2}\left(\int\frac{[\rho_0(E')+\rho_{\mathbf{R}_e}(E')]dE'}{(E-E')^2}\right)^{-1}\\ &=\{c^2\Delta^2/[E_+-\epsilon_b]^2\}\,(dE_+/d\Delta). \end{aligned} \tag{29a}$$

Similarly,

$$I_{ac}(E_+)=\{c^2\Delta^2/[E_+-\epsilon_{ac}]^2\}\,(dE_+/d\Delta). \tag{29b}$$

The polarization ratio $P(\mathbf{b}/\mathbf{ac})$ is simply [comparing Eq. (12c)]

$$P(\mathbf{b}/\mathbf{ac})=[(E_+-\epsilon_{ac})/(E_+-\epsilon_b)]^2(\mid\mu_b\mid^2/\mid\mu_{ac}\mid^2). \tag{29c}$$

For *interchange equivalent pairs*, the situation is slightly different. $\Sigma_2(\mathbf{k}^+=0)$ and $\Sigma_2(\mathbf{k}^-=0)$ are, in this case, no longer the same. From Eq. (25) we note that $\Sigma_2(\mathbf{k}^+=0)$ has a pole at E_+, whereas $\Sigma_2(\mathbf{k}^-=0)$ has a pole at E_-. In other words, *both* E_+ and E_- are *optically allowed* and *uniquely and oppositely polarized*. We have

$$\text{at } E_+,\qquad \Sigma_2(\mathbf{k}^+=0)=\frac{\Delta c^2}{[1-(\Delta/N)f_1(0)]-(\Delta/N)f_2(\mathbf{R}_i)}, \tag{30a}$$

$$\text{at } E_-,\qquad \Sigma_2(\mathbf{k}^-=0)=\frac{\Delta c^2}{[1-(\Delta/N)f_1(0)]+(\Delta/N)f_2(\mathbf{R}_i)}. \tag{30b}$$

The corresponding spectral functions I_b, I_{ac} are found to be

$$\begin{aligned} I_b(E_+)&=\{c^2/[E_+-\epsilon_b]^2\}\{\int[\rho_0(E')+\rho_{\mathbf{R}_i}(E')]dE'/[E_+-E']^2\}^{-1}\\ &=\{c^2\Delta^2/[E_+-\epsilon_b]^2\}\,(dE_+/d\Delta), \end{aligned} \tag{31a}$$

$$\begin{aligned} I_{ac}(E_-)&=\{c^2/[E_--\epsilon_{ac}]^2\}\{\int[\rho_0(E')-\rho_{\mathbf{R}_i}(E')]dE'/[E_--E']^2\}^{-1}\\ &=\{c^2\Delta^2/[E_--\epsilon_{ac}]^2\}\,(dE_-/d\Delta). \end{aligned} \tag{31b}$$

The doublet polarization ratio can be defined, in this case, as

$$P(\mathbf{b}/\mathbf{ac})=[I_b(E_+)\cdot\mid\mu_b\mid^2]/[I_{ac}(E_-)\cdot\mid\mu_{ac}\mid^2],$$

which is simply

$$P(\mathbf{b}/\mathbf{ac})=\frac{[E_--\epsilon_{ac}]^2\cdot\mid\mu_b\mid^2}{[E_+-\epsilon_b]^2\cdot\mid\mu_{ac}\mid^2}\left(\frac{dE_+/d\Delta}{dE_-/d\Delta}\right). \tag{31c}$$

It is noted that, in the limit of small resonance splittings [$E_+\simeq E_-\simeq E(1)$, i.e., when the doublet is not resolved experimentally], Eqs. (29c) and (31c) are all reduced to the familiar Rashba relation [Eq. (12c)].

In summary, we have demonstrated that the general formalism of HR contains, in the limit of infinite dilution, all the "elementary" (or "isolated") cluster states of Koster and Slater in a single expression, with proper weighing factors denoting the probabilities of finding such clusters. It has the appeal of being adaptable to various impurity problems. In the next section, we shall discuss some of the symmetry properties pertaining to the resonance pair problem. While the discussion above, and below, is specifically geared to the naphthalene problem, i.e., a monoclinic crystal with two equivalent molecules per primitive unit cell, it is obviously directly applicable to any crystal in which the interchange group[13b] is of order 2. This happens to be the most common case, by far, for molecular crystals.

B. Symmetry Properties of Resonance Pairs

When considering the symmetry properties of the resonance pairs, it is important to distinguish between translationally equivalent and interchange equivalent pairs.[13] For translationally equivalent pairs, in centrosymmetric crystals like naphthalene, one can show rigorously from group theory that the two molecules of the isolated pair are in *exact* resonance. However, for interchange-equivalent pairs that involve a screw axis or a glide plane, i.e., in naphthalene, there exists only "pseudoresonance," i.e., resonance only within certain approximations.

Consider a centrosymmetric crystal with one *translationally equivalent* pair (all other guests are either remotely located or distributed in a way that will permit us to speak of a "local symmetry" of the guest pair). While such a crystal does not retain its translational symmetry, it *always* retains one inversion center, situated halfway in-between the two molecules. This is obviously true for the nearest neighbor pair. A little reflection will show that it is also true for general translational pairs. This center of inversion assures us that the true mixed crystal solutions are either *gerade* or *ungerade* with respect to inversion. Obviously only the *ungerade* state is optically allowed with respect to a dipole transition from or to the ground state.

The facts that (1) we have a genuine resonance pair and (2) one state is optically allowed and the other forbidden are purely based on group theoretical arguments and, therefore, are independent of the model used. For example, in the crudest oriented gas model, we can write the wavefunctions as

$$\Phi\begin{pmatrix} u \\ g \end{pmatrix} = 2^{-1/2}(\phi_A \pm \phi_B),$$

where ϕ_A, ϕ_B are simply the free-molecule wavefunctions. Notice that in the transport convention[13b] ϕ_B is related to ϕ_A by a translation rather than an inversion. When the *static* interactions between the guest and host are taken into account, we have an "oriented site" model in which ϕ_A and ϕ_B now become the site functions. In the more sophisticated model presented in Sec. II the *dynamic* interactions were introduced. Because of the excitation delocalization, ϕ_A now contains half of all the localized site functions in the crystal; the other half, constituting ϕ_B, is again related by the same inversion. It is expected that if we remove the constraint of short-range interactions associated with the "restricted Frenkel limit," the abovementioned description should still hold. Also, obviously only the ungerade states are "optically allowed."

The one quantity which *does* depend on the model used is the polarization ratio of the allowed component $P(\mathbf{b}/\mathbf{ac})$. In the "oriented gas model" the polarization ratio for the pair is equal to that of one molecule. In the "oriented site model" the polarization ratios for monomer and dimer are still the same (but not equal to that of the free molecule). Finally, when the superexchange effect is introduced, even that is no longer true [compare Eqs. (12c) and (29c)].

Strictly speaking, an interchange equivalent pair is not a "resonance pair." Note that even for an interchange pair fixed in space, the resonance is removed by mutual polarization (a screw axis or a glide plane is not a point symmetry element). However, it is common practice to assume that the mutual guest–guest and guest–host polarization is isotope independent in an isotopically mixed crystal and therefore equal. It is within this context that we speak of interchange pairs as "resonance pairs." The concept[2e] of "ideal mixed crystal" properly contains such an assumption for guest monomers and is easily generalized to dimers.

Once the "resonance" condition is restored, we can always write our wavefunctions as

$$\Phi\begin{pmatrix} \mathbf{b} \\ \mathbf{ac} \end{pmatrix} = 2^{-1/2}(\phi_A \pm \phi_B),$$

whether we use the "oriented gas" or the "oriented site" models. ϕ_A and ϕ_B are either free molecule or site functions. Since ϕ_B is derived from ϕ_A by an interchange operation, the resultant transition moments will be either parallel to the monoclinic axis (**b**) or perpendicular to it (**ac**). In other words, the two dimer lines are uniquely and oppositely polarized. We have shown earlier that this is true even when *dynamic* interactions are introduced in a way consistent with the "restricted Frenkel limit" [compare Eq. (31)]. In the following discussion, we shall explore, from the symmetry point of view, the implication of such an approximation, especially with respect to the polarization and selection rules in the mixed crystal.

Within the "restricted Frenkel limit," the eigenfunctions of the pure crystal take the simple form[20]

$$|\mathbf{k}^{\pm}\rangle = N^{-1/2}[\sum_{\mathbf{R}_\alpha} \exp(i\mathbf{k}\cdot\mathbf{R}_\alpha)\,|\alpha\rangle \pm \sum_{\mathbf{R}_\beta} \exp(i\mathbf{k}\cdot\mathbf{R}_\beta)\,|\beta\rangle], \tag{32a}$$

rather than the most general form

$$|\mathbf{k}^{f}\rangle = N^{-1/2}[A^{f}(\mathbf{k}) \sum_{\mathbf{R}_\alpha} \exp(i\mathbf{k}\cdot\mathbf{R}_\alpha)\,|\alpha\rangle + B^{f}(\mathbf{k}) \sum_{\mathbf{R}_\beta} \exp(i\mathbf{k}\cdot\mathbf{R}_\beta)\,|\beta\rangle] \tag{32b}$$

with

$$|A^{f}(\mathbf{k})|^2 + |B^{f}(\mathbf{k})|^2 = 1 \quad \text{and} \quad f = 1, 2.$$

It is well known that eigenfunctions of a system can only be determined to within an arbitrary phase factor $e^{i\phi}$. If we rewrite Eq. (32a) as

$$|\mathbf{k}^{\pm}\rangle = N^{-1/2}\{\sum_{\mathbf{R}_\alpha} \exp(i\mathbf{k}\cdot\mathbf{R}_\alpha)\,|\alpha\rangle \pm \sum_{\mathbf{R}_\alpha} \exp[i\mathbf{k}\cdot(\boldsymbol{\tau}-\mathbf{R}_\alpha)]\,|\beta\rangle\}, \tag{33a}$$

where $\boldsymbol{\tau}$ is the displacement vector from the corner of the unit cell to the interchange equivalent site, then it is apparent that

$$|\mathbf{k}^{\pm}\rangle = \exp(i\mathbf{k}\cdot\boldsymbol{\tau}/2)\,|\mathbf{k}_p^{\pm}\rangle, \tag{33b}$$

where

$$\begin{aligned}|\mathbf{k}_p^{\pm}\rangle &= N^{-1/2}\{\sum_{\mathbf{R}_\alpha} \exp[i\mathbf{k}\cdot(\mathbf{R}_\alpha-\boldsymbol{\tau}/2)]\,|\alpha\rangle \pm \sum_{\mathbf{R}_\alpha} \exp[i\mathbf{k}\cdot(\boldsymbol{\tau}/2-\mathbf{R}_\alpha)]\,|\beta\rangle\} \\ &= N^{-1/2}[\sum_{\mathbf{R}_n} \exp(i\mathbf{k}\cdot\mathbf{R}_n)\,|\alpha\rangle \pm \sum_{\mathbf{R}_n} \exp(-i\mathbf{k}\cdot\mathbf{R}_n)\,|\beta\rangle],\end{aligned} \tag{33c}$$

where we have replaced $(\mathbf{R}-\boldsymbol{\tau}/2)$ with $\mathbf{R}_n$. The $|\mathbf{k}_p^{\pm}\rangle$ must also be eigenfunctions of the pure crystal. It is also known that, in the absence of magnetic interactions, eigenstates $|\mathbf{k}^{\pm}\rangle$ and $|-\mathbf{k}^{\pm}\rangle$ are doubly degenerate; so are $|\mathbf{k}_p^{\pm}\rangle$ and $|-\mathbf{k}_p^{\pm}\rangle$. Linear combinations can now be constructed to yield symmetric and antisymmetric wavefunctions (with respect to "inversion" at the point $\mathbf{R}=\boldsymbol{\tau}/2$):

$$2^{-1/2}(|\mathbf{k}_p^{+}\rangle \pm |-\mathbf{k}_p^{+}\rangle) = \begin{Bmatrix}(2/N)^{1/2}[\sum_{\mathbf{R}_n} \cos(\mathbf{k}\cdot\mathbf{R}_n)\,|\alpha\rangle + \sum_{\mathbf{R}_n} \cos(\mathbf{k}\cdot\mathbf{R}_n)\,|\beta\rangle] \\ i(2/N)^{1/2}[\sum_{\mathbf{R}_n} \sin(\mathbf{k}\cdot\mathbf{R}_n)\,|\alpha\rangle - \sum_{\mathbf{R}_n} \sin(\mathbf{k}\cdot\mathbf{R}_n)\,|\beta\rangle]\end{Bmatrix}$$

and (34)

$$2^{-1/2}(|\mathbf{k}_p^{-}\rangle \pm |-\mathbf{k}_p^{-}\rangle) = \begin{Bmatrix}(2/N)^{1/2}[\sum_{\mathbf{R}_n} \cos(\mathbf{k}\cdot\mathbf{R}_n)\,|\alpha\rangle - \sum_{\mathbf{R}_n} \cos(\mathbf{k}\cdot\mathbf{R}_n)\,|\beta\rangle] \\ i(2/N)^{1/2}[\sum_{\mathbf{R}_n} \sin(\mathbf{k}\cdot\mathbf{R}_n)\,|\alpha\rangle + \sum_{\mathbf{R}_n} \sin(\mathbf{k}\cdot\mathbf{R}_n)\,|\beta\rangle]\end{Bmatrix}.$$

This is a property peculiar to the eigenfunctions in the "restricted" Frenkel formalism. From the symmetry point of view, we can argue that, in this limit, we are essentially ignoring some of the orientational dependence of the pairwise interactions. In other words, the molecules are being considered temporarily as geometric points occupying the lattice sites. (This is with the reservation that we still distinguish between translationally equivalent molecules and interchange equivalent molecules by, say, painting them in different colors. This distinction is necessary since ϕ_A and ϕ_B are oriented differently in space although they may be related by some symmetry operations. In addition, this distinction also prevents the system from collapsing into a one-molecule-per-unit-cell case with reduced cell dimensions.) It is immediately inferred that, within this limit, as far as the exciton amplitudes are concerned, we *do* have a center of inversion at $\boldsymbol{\tau}/2$, as reflected in the eigenfunctions of Eq. (34). We call this pseudointerchange symmetry "pseudoinversion."

Now, consider an interchange pair at $\mathbf{R}=0$ and $\mathbf{R}=\boldsymbol{\tau}$. Since the "resonance" condition is guaranteed by the isotope independence of the static interactions, the perturbation is totally symmetric with respect to the "pseudoinversion." This assures us that our mixed crystal wavefunctions possess a definite symmetry under such an inversion operation. Furthermore, the optically active states of the pure crystal, $\mathbf{k}^{+}=0$ or $\mathbf{k}^{-}=0$, are *always* symmetric or antisymmetric with respect to the same pseudoinversion. This is so because the eigenfunctions of the $\mathbf{k}=0$ states always have the form of Eq. (32a), even in the general Frenkel case. It is immediately clear that our mixed crystal wavefunctions will be either mixed with $\mathbf{k}^{+}=0$ or $\mathbf{k}^{-}=0$ but *never with both*. In other words, the "symmetric" and "antisymmetric" states have transitions that are uniquely polarized, as indicated in Eq. (30).

It is well known that the pseudoinversion symmetry does not exist in the general Frenkel case, neither in the pure crystal ($\mathbf{k}=0$ is an exception) nor in the mixed crystal. It is expected that interchange pairs in this case will have mixed polarizations. Experimentally, it is probably interesting to investigate how large such an effect is by observing dimers in molecular crystals where long-range interactions are important, such as anthracene.

C. Moment Expansion Method and Sum Rules

The moment expansion method which has been quite useful in the discussion of single impurity states[23] also finds its place in the resonance pair problem. In addition to its practical use in the deep trap limit, this method also serves to demonstrate the interplay of pairwise interactions in forming the resultant resonance pair splitting (*vide infra*).

The integral in the off-diagonal element in Eq. (1) can be expanded in terms of various moments of the off-diagonal density-of-states function $\rho_R(E')$,

$$\int \frac{\rho_R(E')dE'}{(E-E')} = E^{-1}\left(m_R^{(0)} + \frac{m_R^{(1)}}{E} + \frac{m_R^{(2)}}{E^2} + \frac{m_R^{(3)}}{E^3} + \cdots + \frac{m_R^{(n)}}{E^n} + \cdots\right), \tag{35}$$

where

$$m_R^{(n)} = \int (E')^n \rho_R(E')dE'.$$

It is evident from Eq. (2) that the moments can also be written as

$$m_R^{(n)} = N^{-1}[\sum_{\mathbf{k}^+} \epsilon(\mathbf{k}^+)^n \exp(i\mathbf{k}^+\cdot\mathbf{R}) \pm \sum_{\mathbf{k}^-} \epsilon(\mathbf{k}^-)^n \exp(i\mathbf{k}^-\cdot\mathbf{R})]. \tag{36}$$

The sign depends on whether it is a translational pair or an interchange pair. The exciton dispersion relation is especially simple within the "restricted Frenkel limit,"

$$\epsilon(\mathbf{k}^\pm) = \sum_{\mathbf{R}_\alpha} M_\alpha \exp(i\mathbf{k}\cdot\mathbf{R}_\alpha) \pm \sum_{\mathbf{R}_\beta} M_\beta \exp(i\mathbf{k}\cdot\mathbf{R}_\beta), \tag{37}$$

where $\mathbf{M}_\alpha$ and $\mathbf{M}_\beta$ are translationally equivalent and interchange equivalent interactions, respectively. If we substitute Eq. (37) into Eq. (36) we find that

$$m_R^{(n)} = \sum_{\{n\}} M_1 M_2 M_3 \cdots M_n, \tag{38}$$

where M_1, M_2, M_3, $\cdots$, M_n are pairwise interactions between the molecule at the origin and the molecules at $\mathbf{R}_1$, $\mathbf{R}_2$, $\mathbf{R}_3$, $\cdots$, $\mathbf{R}_n$, respectively. These n vectors must satisfy the condition that $\mathbf{R}_1+\mathbf{R}_2+\mathbf{R}_3+\cdots+\mathbf{R}_n=\mathbf{R}$. The summation $\sum_{\{n\}}$ must be carried over all possible sets of M's that satisfy the above relation. A simple topological interpretation of Eq. (38) would be the following: Given n steps, determine all the possible routes in going from one guest of the resonance pair to the other. The rule is such that we can move from one molecule to the other if they are connected via a nonnegligible interaction; form the product of all the M's involved in each route and sum over all the possible products, one for each possible route. It is easy to see that $m_R^{(0)}=0$, $m_R^{(1)}=M_R$, etc. Equations (35) and (38) will enable us to examine explicitly how the resonance pair splittings depend on the pairwise interactions and the trap depth.

A sum rule can also be derived by noting that

$$\sum_{\mathbf{R}_\alpha} \int \frac{\rho_{R_\alpha}(E')dE'}{(E-E')} = N^{-1}\left(\sum_{\mathbf{k}^+} \frac{\sum_{R_\alpha} \exp(i\mathbf{k}^+\cdot\mathbf{R}_\alpha)}{E-\epsilon(\mathbf{k}^+)} + \sum_{\mathbf{k}^-} \frac{\sum_{R_\alpha} \exp(i\mathbf{k}^-\cdot\mathbf{R}_\alpha)}{E-\epsilon(\mathbf{k}^-)}\right)$$

$$= \tfrac{1}{2}\{[E-\epsilon(\mathbf{k}^+=0)]^{-1} + [E-\epsilon(\mathbf{k}^-=0)]^{-1}\} - \int \frac{\rho_0(E')dE'}{E-E'}. \tag{39a}$$

Similarly,

$$\sum_{\mathbf{R}_\beta} \int \frac{\rho_{R_\beta}(E')dE'}{(E-E')} = N^{-1}\left(\sum_{\mathbf{k}^+} \frac{\sum_{R_\beta} \exp(i\mathbf{k}^+\cdot\mathbf{R}_\beta)}{E-\epsilon(\mathbf{k}^+)} - \sum_{\mathbf{k}^-} \frac{\sum_{R_\beta} \exp(i\mathbf{k}^-\cdot\mathbf{R}_\beta)}{E-\epsilon(\mathbf{k}^-)}\right)$$

$$= \tfrac{1}{2}\{[E-\epsilon(\mathbf{k}^+=0)]^{-1} - [E-\epsilon(\mathbf{k}^-=0)]^{-1}\}. \tag{39b}$$

In deriving these rules, we have used the closure properties of the pure crystal eigenfunctions. Furthermore, when the resonance pair splitting is small compared to the trap depth, we can expand Eq. (1b) at $E(1)$, the monomer energy. Equation (1b) becomes[24]

$$\Delta[E-E(1)] \int [\rho_0(E')dE'/(E(1)-E')^2] = \pm\Delta \int [\rho_R(E')dE'/(E-E')],$$

or

$$[E-E(1)] = \pm \frac{\int [\rho_R(E')dE'/(E-E')]}{\int [\rho_0(E')dE'/(E(1)-E')^2]}. \tag{40}$$

We concentrate on the *plus* state and put $E_+-E(1)=S_R$. We also assume that the right-hand side of Eq. (40) is slow varying and hence can be approximated by substituting $E(1)$ for E_+. We have, from Eq. (3a),

$$S_R=\frac{\int[\rho_R(E')dE'/(E(1)-E')]}{\int[\rho_0(E')dE'/(E(1)-E')^2]}$$
$$=\Delta^2[dE(1)/d\Delta]\int[\rho_R(E')dE'/(E(1)-E')]. \tag{41}$$

From Eqs. (39) and (41), we have the *sum rule*,

$$\sum_{R_\alpha} S_{R_\alpha}=\Delta^2[dE(1)/d\Delta]\left(\tfrac{1}{2}\{[E(1)-\epsilon(\mathbf{k}^+=0)]^{-1}+[E(1)-\epsilon(\mathbf{k}^-=0)]^{-1}\}-\Delta^{-1}\right)$$

and

$$\sum_{R_\beta} S_{R_\beta}=\Delta^2[dE(1)/d\Delta]\tfrac{1}{2}\{[E(1)-\epsilon(\mathbf{k}^+=0)]^{-1}-[E(1)-\epsilon(\mathbf{k}^-=0)]^{-1}\}. \tag{42}$$

Notice that in the deep trap limit we have the expected results,

$$\sum_{R_\alpha} S_{R_\alpha}=\sum_{\alpha} M_\alpha$$

and

$$\sum_{R_\beta} S_{R_\beta}=\sum_{\beta} M_\beta.$$

III. RESONANCE PAIRS AND INTERACTIONS IN $^1B_{2u}$ NAPHTHALENE

A. Pairwise Interactions and Dimer Splittings

As shown in the previous sections, resonance pair splittings (the S_R's) become equal to the pairwise interactions (the M_R's) in the deep trap limit. Experimental results in this limit will, therefore, yield both the sign and the magnitude of the latter quantities. However, in practice, there are two difficulties: (1) The deep trap limit cannot be readily reached by isotopic substitutions, such as in the present case of the naphthalenes (maximum trap depth = 115 cm^{-1}). (2) Within the restricted Frenkel theory, one can use the polarization data to distinguish between translationally equivalent and interchange equivalent dimers; however, within the same category, there is no simple criterion for assigning a particular absorption to a particular dimer. The second difficulty can be tackled by reducing the trap depth and introducing the quasi-resonance effects. As our results will later demonstrate, at least partial assignments can thus be achieved. As for the first difficulty, other related data, such as density-of-states functions, single impurity levels, etc., will have to be used as criteria if the deep trap data are not available.

The fact that only a few absorption lines attributable to resonance pairs were observed[4] in naphthalene-h_8 in naphthalene-d_8 indicates that intermolecular interactions in the $^1B_{2u}$ excited state do fall off very rapidly. Restricted Frenkel theory is thus expected to be adequate. When intermolecular distances alone are considered, the leading interaction terms are those listed in Table I. The corresponding exciton dispersion relation can be written as[25a]

$$\epsilon(\mathbf{k}^\pm)=2M_a\cos(\mathbf{k}\cdot\mathbf{a})+2M_b\cos(\mathbf{k}\cdot\mathbf{b})+2M_c\cos(\mathbf{k}\cdot\mathbf{c})$$
$$+2M_{a+c}[\cos(\mathbf{k}\cdot\mathbf{a})\cos(\mathbf{k}\cdot\mathbf{c})-\sin(\mathbf{k}\cdot\mathbf{a})\sin(\mathbf{k}\cdot\mathbf{c})]$$
$$\pm(4M_{12}\cos[\mathbf{k}\cdot(\mathbf{a}/2)]\cos[\mathbf{k}\cdot(\mathbf{b}/2)]+4M_{12'}$$
$$\times\{\cos(\mathbf{k}\cdot\mathbf{c})\cos[\mathbf{k}\cdot(\mathbf{a}/2)]\cos[\mathbf{k}\cdot(\mathbf{b}/2)]$$
$$-\sin(\mathbf{k}\cdot\mathbf{c})\sin[\mathbf{k}\cdot(\mathbf{a}/2)]\cos[\mathbf{k}\cdot(\mathbf{b}/2)]\}), \tag{43}$$

where M_{12} designates the pair interaction for $\mathbf{R}=\frac{1}{2}(\mathbf{a}+\mathbf{b})$, $M_{12'}$ for $\mathbf{R}=\frac{1}{2}(\mathbf{a}+\mathbf{b})+\mathbf{c}$, etc.

A trial and error method can be devised to obtain several sets of M's consistent with Hanson's[4] experimental data by using Eq. (43) and Eqs. (1) and (2). In doing this, it is especially gratifying that only one interchange equivalent dimer was identified spectroscopically in $^1B_{2u}$ naphthalene and obviously assigned to the nearest-neighbor pair, $\mathbf{R}=\frac{1}{2}(\mathbf{a}+\mathbf{b})$. This fact not only removes any possible ambiguities concerning the interchange equivalent dimers but also enables us to distinguish one subgroup of translationally equivalent dimers from the other as will be clear from the following discussions. Alongside the large M_{12} term we also assigned a small $M_{12'}$ term, adjusted such that their sum gives the right Davydov splitting.[2f]

To proceed with our calculations, we assigned, quite arbitrarily, the four known translationally equivalent dimer splittings: -7.9, -5.1, -3.3, and 3.7 cm^{-1} to the four possible dimers ($\mathbf{R}=\mathbf{a}$, $\mathbf{R}=\mathbf{b}$, $\mathbf{R}=\mathbf{c}$, and $\mathbf{R}=\mathbf{a}+\mathbf{c}$). In principle, there are 24 possible assignments, each representing a distinct physical situation. However, within our simplified model where the interactions have been truncated, the interchange of M_c and M_{a+c} fails to produce a new physical entity.[25b]

TABLE I. Possible assignments of pairwise interactions and dimer splittings in the $^1B_{2u}$ excited state of naphthalene.

			Set 1[d]				Set 2				Set 3			
Classification	Position[c]	Å	M[e]	S_{calc}[f]	$S_{ass'd}$[g]	δ[h]	M	S_{calc}	$S_{ass'd}$	δ	M	S_{calc}	$S_{ass'd}$	δ
IE pairs[a]	$\frac{1}{2}$(a+b)	5.10	18.0	15.0	15.3	−3.0	18.0	14.7	15.3	−3.3	18.0	14.2	15.3	−3.8
	$\frac{1}{2}$(a+b)+c	7.89	2.0	...	...	...	1.0	...	...	...	1.0	...	...	...
TE pairs[b]	a	8.24	{−0.6}[i]	−5.0	−5.1	−4.4	{−4.3}	−7.5	−7.9	−3.2	{−1.2}	−4.8[j]	−5.1	−3.6[j]
	b	6.00	{−3.9}	−8.0	−7.9	−4.1	{1.9}	−3.2	−3.3	−5.1	{1.6}	−3.4	−3.3	−5.0
	c	8.66	{6.1}	4.0	3.7	−2.1	{−6.1}	−5.2	−5.1	0.9	{−8.9}	−7.9	−7.9	1.0
	a+c	7.96	{−3.7}	−3.5	3.3	0.2	{6.0}	4.0	3.7	−2.0	{6.0}	4.1	3.7	−1.9
Translational shift			−4.2				−5.0				−5.0			

[a] Interchange equivalent pairs.
[b] Translationally equivalent pairs.
[c] The positions of the second molecule of the pair with respect to the first which is at the origin.
[d] All in units of cm^{-1}.
[e] M = pairwise interactions.
[f] S_{calc} = calculated energies of the plus state of dimer − calculated energy of the monomer.
[g] $S_{ass'd}$ = observed energy of the plus state of dimer − observed energy of the monomer.
[h] $\delta = (S_{calc} - M)$ or the exciton superexchange term, see text.
[i] Braces here indicates that two rows can be exchanged. See discussion in the text.
[j] These values were misquoted in Phys. Rev. Letters **25**, 1030 (1970).

TABLE II. Other possible assignments of pairwise interactions and dimer splittings[a] (rejected because of poor agreements with monomer energies and density-of-states function).

			Set 4				Set 5				Set 6			
Classification	Position	Å	M	S_{calc}	$S_{ass'd}$	δ	M	S_{calc}	$S_{ass'd}$	δ	M	S_{calc}	$S_{ass'd}$	δ
IE pairs	$\frac{1}{2}$(a+b)	5.10	21.0	14.5	15.3	−6.5	21.3	15.0	15.3	−6.0	22.0	15.0	15.3	−7.0
	$\frac{1}{2}$(a+b)+c	7.89	−1.0	...	...	...	−1.5	...	...	...	−2	...	...	...
TE pairs	a	8.24	{−0.1}	−5.0	−5.1	−4.9	{−3.5}	−8.0	−7.9	−4.5	{12.0}	3.7	3.7	−8.3
	b	6.00	{10.7}	4.0	3.7	−6.7	{11.2}	3.5	3.7	−7.7	{2.4}	−3.0	−3.3	−5.4
	c	8.66	{−8.8}	−7.5	−7.9	1.3	{−6.0}	−5.5	−5.1	0.9	{−7.0}	−5.5	−5.1	1.5
	a+c	7.96	{−2.8}	−3.0	−3.3	−0.2	{−3.0}	−3.3	−3.3	−0.3	{−10.1}	−8.3	−7.9	1.8
Translational shift			−2.0				−2.6				−5.4			

[a] All headings here are similar to those of Table I.

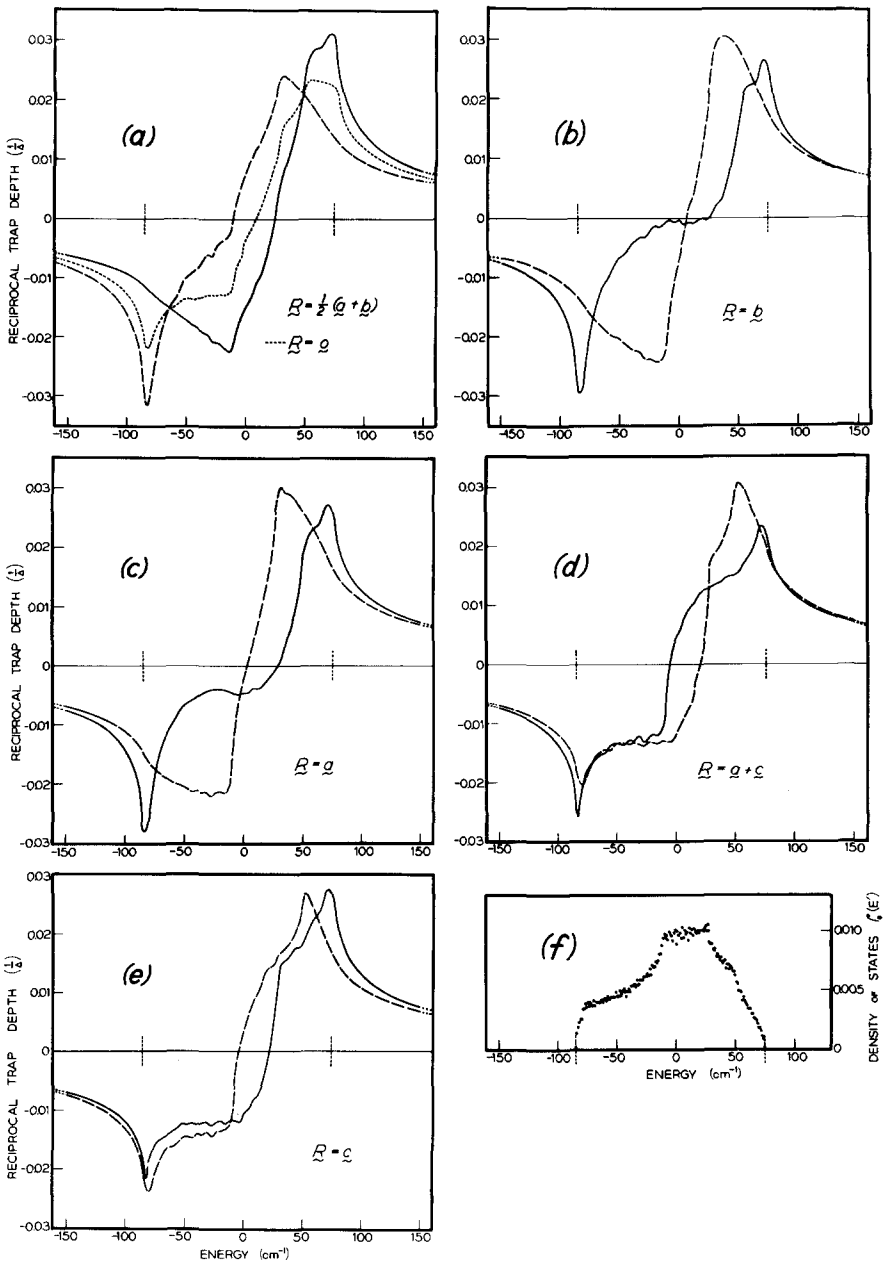

FIG. 6. (a) to (e): The $^1B_{2u}$ naphthalene dimer energies plotted as functions of the reciprocal trap depth $(1/\Delta)$. Solid curves are for E_+ and dashed curves are for E_-. Notice that the corresponding curve for monomer energy, $E(1)$, is also included (dotted line) in Fig. (a). The intermolecular exciton interaction parameters used here are those of Set 1 in Table I. The two vertical dotted lines represent the band edges which happen to coincide with the two Davydov components. (f) The density-of-states function plotted with the same parameters.

Furthermore, because of the large M_{12} involved, the interchange of M_a and M_b also results in *roughly* the same result.[15b] When these two facts are taken into account, we are left with only *six* possible assignments. A total of 16 000 points in the Brillouin zone were included in the calculation. The convergence was very good. Normally four or five iterations are needed before we have a satisfactory set.

All above six sets are listed in Tables I and II. It can be seen that in each case "quasiresonance" interactions between the host and the guest are not negligible. The first-order calculations by Hanson[4a] are certainly inadequate. The "quasiresonance" effects on the dimer splittings (as shown by the δ's in Tables I and II) are especially pronounced in the case of the **a** and **b** dimers. Due to the large interchange interaction term, M_{12}, and hence the large degree of excitation delocalization to the host, the final dimer splittings are determined as much by the indirect couplings via the host molecules as by the direct coupling between the guest molecules themselves. In analogy to the spin delocalization phenomena in the discussion of magnetic states[26] of solids, we call this effect "exciton superexchange."

To illustrate this superexchange effect, we have calculated the lhs of Eq. (3) as a function of energy shown in Fig. 6. Notice that, according to Eq. (3), such curves give directly E_+ (the solid curves) and E_-

(the dotted curves) as a function of reciprocal trap depths. The interaction parameters used were those of Set 1 in Table I. The E_+ and E_- curves in Figs. 6(a) and 6(e) can be described as "well behaved" in the sense that, for all the bound states (outside the band), E_+ is always higher (lower) in energy when the interaction between the guests is positive (negative). In other words, S always has the same sign as M, although the magnitude may be different. An extreme case is illustrated by the curves in Figs. 6(b) and 6(c). On the one hand, bound states below the band are marked by a splitting much larger than the direct coupling and, on the other, level crossing actually occurs for states above the band. S can be different from M both in magnitude and sign. The curves in Fig. 6(d) are considered as a border line case.

In Figs. 7(a) and 7(b), more conventional energy vs trap-depth plots are given for $\mathbf{R}=\mathbf{a}$ and $\mathbf{R}=\frac{1}{2}(\mathbf{a}+\mathbf{b})$. Again it shows the dramatic superexchange effect on the $\mathbf{a}$ dimer splitting: At a trap depth of $+200$ cm^{-1}, E_+ is still higher in energy than E_- although $M=-0.6$ cm^{-1}!

It is concluded that the superexchange effects must be carefully checked in interpreting the dimer spectra. As shown in our calculations, the pairwise interactions inferred from simple first-order arguments may be erroneous both in magnitude and in sign. On the other hand, because of the specific nature of the superexchange interactions, this effect can now be utilized to assign a given spectral feature to a given pair, as is discussed in detail below.[27]

B. Exciton Superexchange and Moment Expansion Method

To gain some insights about the nature of exciton superexchange, we consider here a simple model, consisting of two guests and two hosts. We assume that the specific guest–guest and host–host interactions are small whereas guest–host interactions are large. Referring to the naphthalene crystal structure, we notice that this simple model closely represents, say, a resonance pair mode of one molecule at the origin and another at $\mathbf{R}=\mathbf{a}$ together with two host molecules at $\mathbf{R}=1/2(\mathbf{a}+\mathbf{b})$ and $\mathbf{R}=1/2(\mathbf{a}-\mathbf{b})$. Consistent with our assumption, we put $M_a=M_b=0$. The secular determinant has the following form:

$$\begin{vmatrix} G-E & 0 & M_{12} & M_{12} \\ 0 & G-E & M_{12} & M_{12} \\ M_{12} & M_{12} & H-E & 0 \\ M_{12} & M_{12} & 0 & H-E \end{vmatrix} = 0,$$

where G and H are excitation energies for guest and host, respectively.

General solutions to matrices of this type have been discussed before.[28] In the present simple case the four

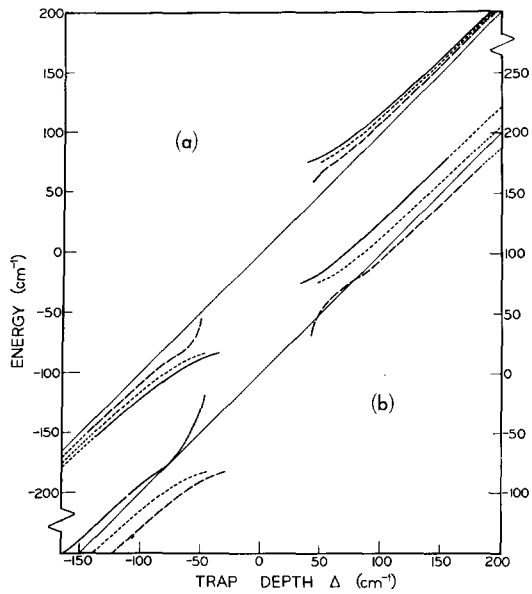

FIG. 7. The $^1B_{2u}$ dimer energies plotted as functions of the trap depth (Δ). Solid, dashed, and dotted curves are for E_+, E_-, and $E(1)$, respectively. The dimer separations are: (a) $\mathbf{R}=\mathbf{a}$ and (b) $\mathbf{R}=\frac{1}{2}(\mathbf{a}+\mathbf{b})$. The interaction parameters used here are the same as those in Fig. 6.

eigenstates have energies given by

$$E_+^H = H+\tfrac{1}{2}\Delta+\tfrac{1}{2}(\Delta^2+16M_{12}^2)^{1/2},$$
$$E_-^H = H,$$
$$E_-^G = G,$$
$$E_+^G = G-\tfrac{1}{2}\Delta-\tfrac{1}{2}(\Delta^2+16M_{12}^2)^{1/2},$$

with $\Delta=G-H$ as trap depth. The corresponding eigenfunctions are

$$\Psi_+^H = 2^{-1/2}[(1-\sigma)^{1/2}(\phi^{H_1}+\phi^{H_2})+\sigma(\phi^{G_1}+\phi^{G_2})],$$
$$\Psi_-^H = (1/\sqrt{2})(\phi^{H_1}-\phi^{H_2}),$$
$$\Psi_-^G = (1/\sqrt{2})(\phi^{G_1}-\phi^{G_2}),$$
$$\Psi_+^G = 2^{-1/2}[-(1-\sigma)^{1/2}(\phi^{G_1}+\phi^{G_2})+\sigma(\phi^{H_1}+\phi^{H_2})],$$

where ϕ^{G_1}, ϕ^{G_2}, ϕ^{H_1}, and ϕ^{H_2} are localized excitation functions for guests (G_1 and G_2) and host (H_1, H_2), respectively, and

$$\sigma = \frac{2M_{12}}{\{4M_{12}^2+[\frac{1}{2}(\Delta^2+16M_{12}^2)^{1/2}-\frac{1}{2}\Delta]^2\}^{1/2}}.$$

The exciton superexchange (es) term, which is exactly $1/2(E_+^G-E_-^G)$ in this case, because the 1st-order splitting is zero, is simply

$$\delta_{es} = -\tfrac{1}{4}\Delta-\tfrac{1}{4}(\Delta^2+16M_{12}^2)^{1/2}.$$

For example, in a mixed crystal of $C_{10}H_8$ in $C_{10}D_8$ ($\Delta=-115$ cm^{-1} and $M_{12}\simeq 20$ cm^{-1}), this quantity amounts to

$$\delta_{es}\simeq -6 \text{ cm}^{-1},$$

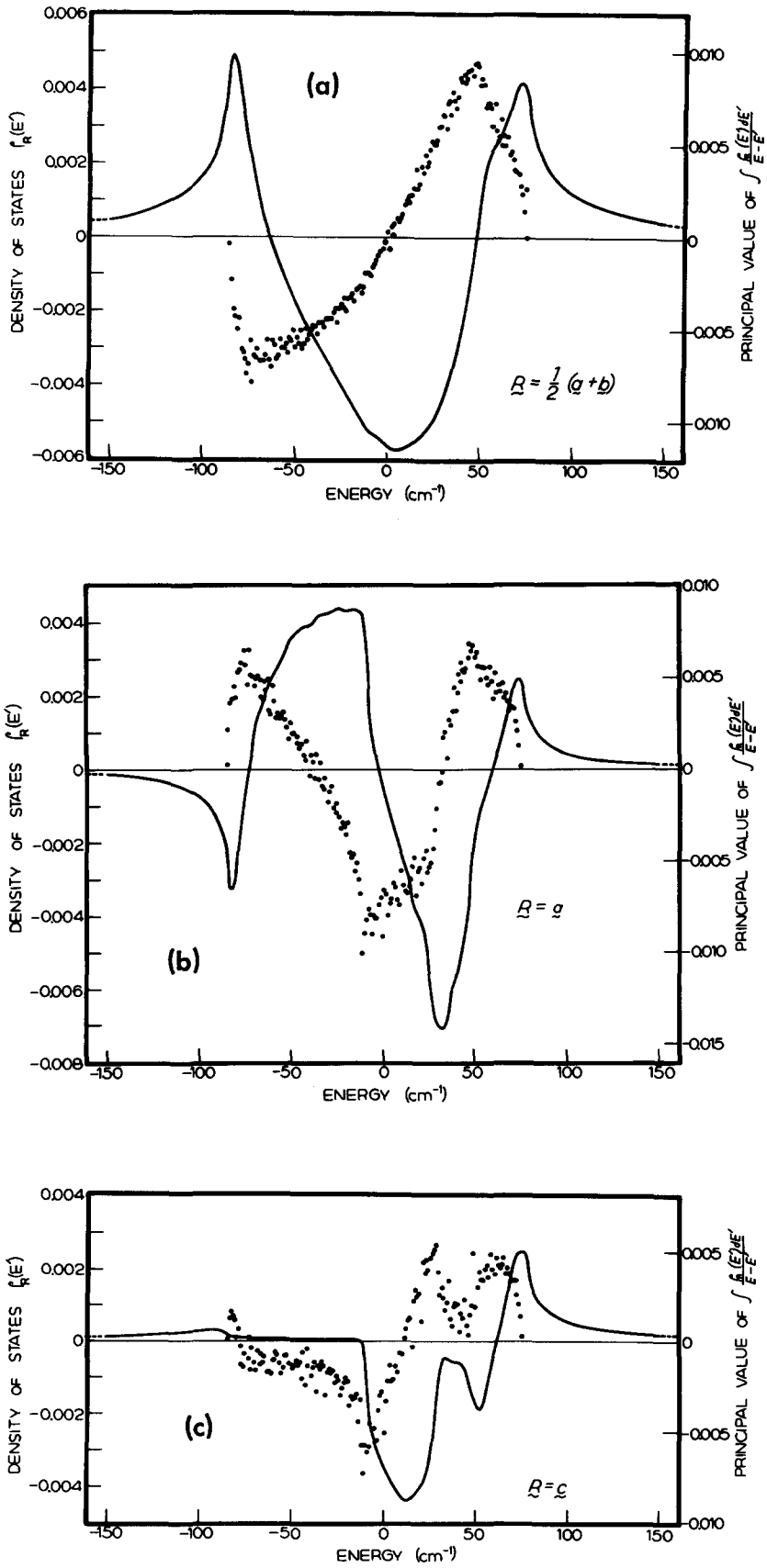

FIG. 8. The off-diagonal density-of-states function $\rho_R(E')$ (dots) and the corresponding integral $\int[\rho_R(E')dE'/(E-E')]$. The interaction parameters used here are the same as those in Fig. 6. Notice that for $\mathbf{R}=\mathbf{a}$ the integral is positive for positive energy although M_a is negative. This is why in Figs. 6 and 7 we have "level crossing" for the **a** dimer in this region.

TABLE III. Various moments of $\rho_R(E')$ as calculated from Set 1 for resonance pairs in crystalline naphthalene.

Resonance pairs	$m_R^{(1)}$	$m_R^{(2)}\times10^{-2}$	$m_R^{(3)}\times10^{-4}$	$m_R^{(4)}\times10^{-6}$	$m_R^{(5)}\times10^{-8}$	$m_R^{(6)}\times10^{-10}$	$m_R^{(7)}\times10^{-12}$	$m_R^{(8)}\times10^{-14}$	$m_R^{(9)}\times10^{-16}$
$\frac{1}{2}$(a+b)	17.8	−1.69	5.74	−1.27	2.40	−0.81	1.14	−0.49	0.60
a	−0.6	5.93	−0.99	2.70	−0.76	1.31	−0.51	0.68	−0.32
b	−3.9	6.50	−1.75	2.99	−1.02	1.45	−0.62	0.76	−0.38
c	6.1	1.40	1.58	0.59	0.54	0.27	0.19	0.14	0.07
a+c	−3.7	1.38	−0.58	0.90	−0.24	0.50	−0.15	0.29	−0.11

which compares well with more exact results of Tables I and II. The extent of delocalization can also be estimated by evaluating σ^2:

$$\sigma^2\simeq 0.1,$$

a relatively small quantity indeed.

We have discussed above a simple manifestation of exciton superexchange with a four-body model. The situation is, of course, more complicated if the whole crystal is considered. Here the moment expansion method discussed in Sec. II.C is most appropriate. In Fig. 8 we again use our first set of parameters to plot ρ_R, the off-diagonal density-of-states function, and the corresponding integral $\int[\rho_R(E')dE'/(E-E')]$. The same electrostatic analogy[29] can be made as in the case of ρ_0 (the pure crystal density-of-states function). If ρ_R is considered as the charge distribution (both positive and negative charges are present in this case), then the integral is nothing but the potential. Through Eq. (35), this potential can be expanded in powers of $1/E$. The leading term, $m_R^{(1)}/E^2$ [since $m_R^{(0)}/E$ is invariably equal to zero], gives the first-order splitting and the higher-order terms will be the "superexchange" contributions.

The first term in the superexchange contributions to the dimer splitting is $m_R^{(2)}/E^3$. According to Eq. (38), we can write down the following expressions for various dimers in naphthalene:

a dimer	$m_a^{(2)}=2M_{12}^2+2M_cM_{a+c}$,
b dimer	$m_b^{(2)}=2M_{12}^2+2M_{12'}^2$,
c dimer	$m_c^{(2)}=2M_aM_{a+c}+4M_{12}M_{12'}$,
a+c dimer	$m_{a+c}^{(2)}=2M_aM_c+4M_{12}M_{12'}$,
$\frac{1}{2}$(**a+b**) dimer	$m_{1/2(a+b)}^{(2)}=2M_{12}M_a+2M_{12}M_b+M_{a+c}M_{12'}+2M_{12'}M_c$.

It is immediately clear that **a** and **b** dimers have large superexchange contributions due to M_{12}^2, whereas **c** and **a+c** dimers are relatively uneffected. These results are qualitatively in agreement with our calculated results in Tables I and II.

We have tabulated in Table III some of the lower-order superexchange contributions for naphthalene-h_8 in naphthalene-d_8. It is exactly this poor convergence in the power expansion (or equivalently large superexchange contribution) that made it necessary in this case to use the exact method [Eq. (3)] in interpreting dimer data for $^1B_{2u}$ naphthalenes. Note, for instance, that for the $\frac{1}{2}$(**a+b**) pair the third moment is larger than the second, which is reasonable due to the large size of the $2M_{12}^3$ term.

C. Pairwise Interactions, Pure Crystal Density of States Function, and Monomer Energies

As far as comparisons with dimer splittings in naphthalene-h_8 in naphthalene-d_8 are concerned, our above-mentioned six sets of pair interactions are equally good. Figure 9 shows how we generate these six sets of parameters from Hanson's data.[4] It should be pointed out that each set predicts very different dimer splittings at the deep trap limit (where $S=M$). Therefore, if deep trap data were available for naphthalene, we could readily distinguish between dimers in the **ab** plane and dimers outside of it, thanks to the large M_{12} term (compare M and S values in Tables I and II). However, the distinction between **a** and **b** dimers (or between the **a+c** and **c** dimers[25b]) would still require very accurate data and also more refined calculations with more interactions. The important point demonstrated here is how one can use the superexchange effect to aid the assignments of dimer data, which would otherwise be very difficult.

Physically, we have a situation where one can apply an "anisotropic" environmental perturbation (i.e., the superexchange) to the coupled oscillators (i.e., the dimer). Depending on the magnitude of the anisotropy, partial or total assignments can be achieved. Another important point is that all six sets predict a very small translational shift. The experimental (hot band) translational shift of about -2 ± 10 cm^{-1} for $^1B_{2u}$ naphtha-

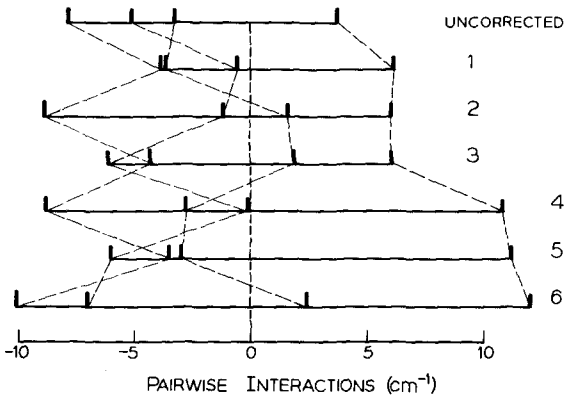

FIG. 9. A schematic diagram for the pairwise interactions tabulated in Table I and II. The top one represents the dimer lines of Hanson.[4a] The dotted lines connect all the pairwise interactions generated from the same dimer lines due to different assignments (Sets 1–6 in Tables I, II). This diagram also represents for each assignment the possible dimer absorption lines in the deep-trap limit, with the monomer line at the origin ($E=0$).

lene[2f] is thus independently verified from the dimer data. The large discrepancy Hanson[4] observed is simply a result of not correcting for the superexchange effect. In fact, we feel justified to place this important quantity in an even narrower bracket of -4.5 ± 4 cm^{-1}.

In an attempt to narrow down the choice among possible interaction parameters, we have calculated both the pure crystal density-of-states function and the single-impurity levels for all the six sets in Tables I and II. For single-impurity levels, 16 000 points in the Brillouin zone were used as before, whereas for density-of-states functions the number was increased to 432 000, with a 1-cm^{-1} mesh. These results are shown in Figs. 10(b)–10(d) and Figs. 11(a)–11(c). Figure 10(a) shows the density-of-states function using the uncorrected parameters. The agreement is rather poor. On the contrary, the three sets included in Table I give excellent agreement with the experimental hot-band data. The other three sets which all contain one large positive (translationally equivalent) interaction term ($\sim$10 cm^{-1}) give density-of-states functions that are well extended beyond the higher Davydov components, as shown in Figs. 11(a)–11(c). From the density-of-states functions alone, the experimental evidence seems to discriminate against the last three sets.

It has been argued[2f,23b] that, because of the unknown phonon contribution to the density-of-states function, the hot-band results are not without uncertainties. It is also known[2f,23b] that investigations on single impurity levels are void of such complications. To have an independent criterion we have thus calculated the monomer energies for all these six sets. The results are shown in Fig. 12. It should be noted that we have lined up the lowest Davydov components found experimentally with those predicted by each of the six sets of parameters. Since the *ac* component of the host can be determined experimentally with great accuracy, the experimental guest levels plotted in Fig. 12 are all measured relative to the *ac* component of the host. This scheme is slightly different from the previous one (Figs. 10, 11) which uses the band center as the common datum. This was done to avoid any prejudice with regard to the *absolute* position of the band center and also to conform with previous work on the same subject.[2f,23b]

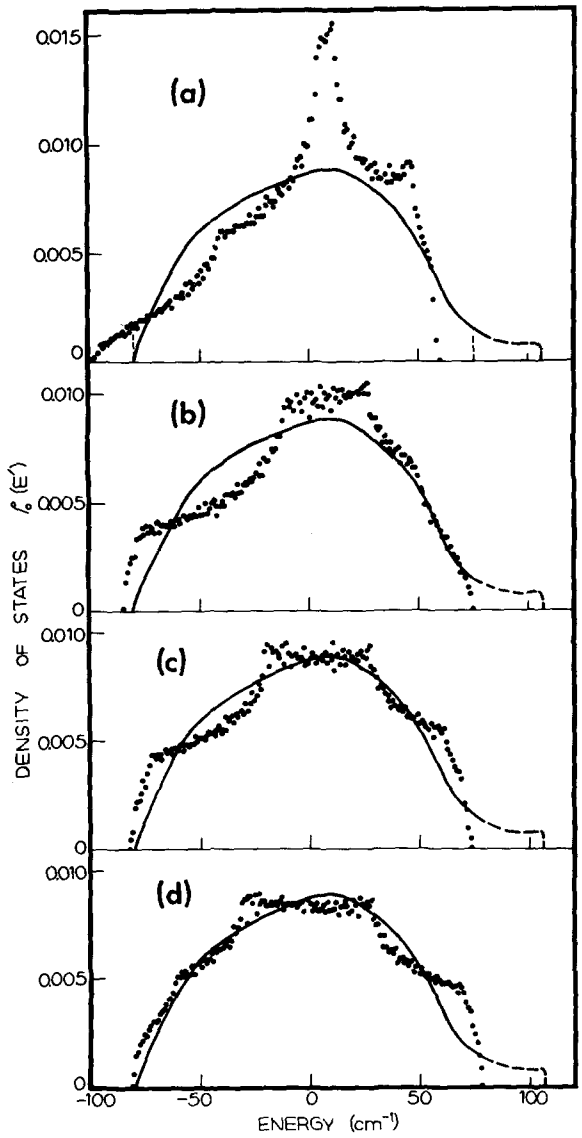

FIG. 10. Density-of-states functions calculated with the interaction parameters given by (a) Hanson,[4a] (b) Set 1, (c) Set 2, (d) Set 3. The last three sets are those in Table I. The superimposed solid curve is the experimental[2d] (hot-band) density-of-states function (dashed part uncertain due to experimental difficulties). In each case both the experimental and the calculated band centers are placed at the origin. The vertical dotted lines in (a) are the *experimental* Davydov components. For (a), (b), (c), and (d) the calculated Davydov components coincide with the upper and lower band edges.

From Fig. 12 we can see that for impurities below the band, there is actually very little difference among all six sets. However, for impurities above the band, only the first three sets give bound states for the trap depths investigated experimentally. In the region where three bound states were observed experimentally, none of the last three sets predicts any bound states. This second criterion therefore unequivocally rules out these last three sets.

By the above process of successive elimination, we are left with *three* sets of intermolecular interaction parameters which agree with: (1) Davydov splitting, (2) the experimental (hot-band) density-of-states function, (3) the monomer energies, (4) the resonance pair data. In other words, as far as experimental data are available and can be checked, our three sets are consistent with them all. To further discriminate among these sets additional resonance pair data for other trap depths would certainly be helpful. As for the deep trap limit, suitable vibronic bands may provide the answers.[30]

Although our search for pairwise interactions is incomplete, nevertheless, we can set some limits within

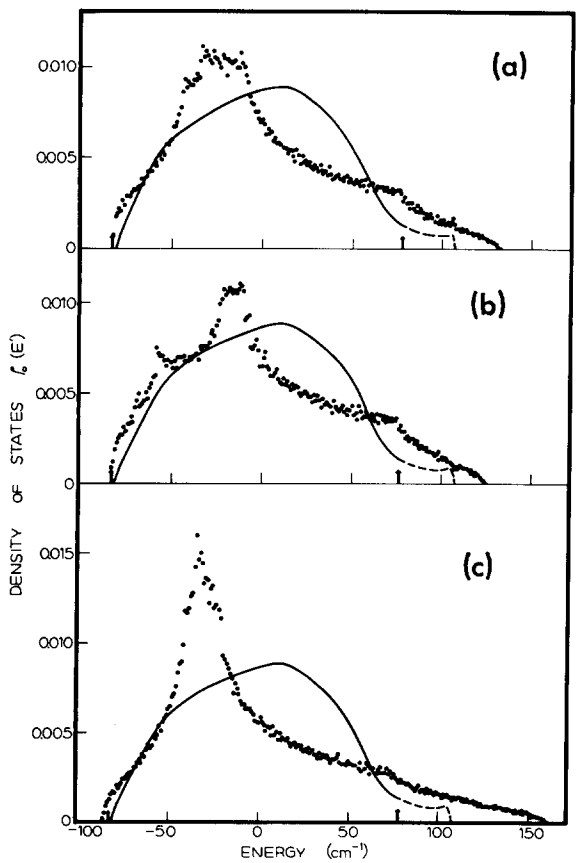

FIG. 11. Density-of-states function calculated with the interaction parameters given by (a) Set 4, (b) Set 5, (c) Set 6 in Table II. The conventions used here are the same as those of Fig. 10. Since the calculated Davydov components do not coincide with the band edges they are shown here as solid vertical arrows.

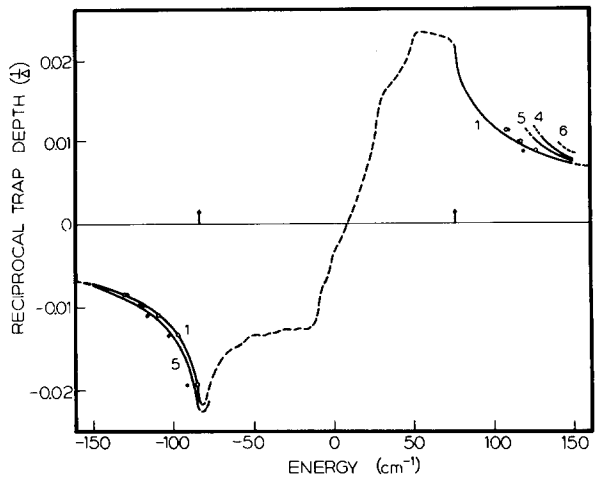

FIG. 12. The monomer energies plotted as a function of the reciprocal trap depth $(1/\Delta)$. The solid circles are the experimental values[2f] and the open circles are the values calculated in Ref. 2(f), using the experimental density-of-states function. The numbers given correspond to the set numbers (Table I and II). Since the results from Sets 1 to 3 are quite similar, only the curve for Set No. 1 is shown. For impurities below the band the results for all sets are quite similar and bracketed within the curves for Set 1 and Set 5. For impurities above the band, Sets 4 to 6 yield no bound states in the region investigated experimentally, and this is indicated by dotted lines in the figure. The arrows are the **ac** and **b** Davydov components calculated from Set 1. Notice that the conventions used here are different from those in Figs. 10 and 11. Here the calculated and experimental bands are superimposed at the **ac** Davydov component (see text) rather than at the band center.

which the actual density-of-states function must lie. Figure 13 shows such limits as defined by the density-of-states function of Fig. 10(b)–10(d). It can be seen that the experimental (hot-band) density-of-states function *does* lie within these limits,[31a] considering experimental errors. The fact that *all* three sets yield density-of-states functions similar to the experimental one is gratifying. It should be noted that had any such set yielded a different density-of-states function, the choice among the sets would be difficult and the validity of the experimental density-of-states function could not be checked conclusively. This is due to the fact that phonons have practically no effect on impurity levels but they always contribute to a hot-band transition to some extent. Any discrepancies in the density-of-states function observed in this case would have been attributable to phonon participation. In reality our experimental evidence indicates otherwise. Figure 13 clearly demonstrates that phonons make *little or no* contribution to the corrected band-to-band transition in $^1B_{2u}$ naphthalene. This is probably why the experimental density-of-states function has been, up till now, the best one available: It has been successful in accounting for the monomer energies and even for heavily doped mixed crystals,[5,6] despite all the doubts concerning the role played by the phonons.[31b]

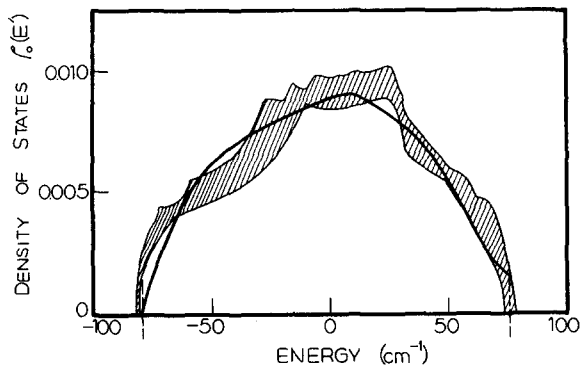

FIG. 13. Calculated and experimental $^1B_{2u}$ naphthalene exciton density-of-states functions. The cross-hatched area represents the outer bounds of a superposition of the three functions derived from the three sets in Table I (compare Fig. 10). The solid curve is the experimental density-of-states function,[2d] with the high-energy edge truncated due to large experimental uncertainties. Dashed lines represent the experimental Davydov components. The calculated and experimental curves have been superimposed at the band center (E-0).

Finally, we would like to add some comments on the sum rule developed in Sec. II.c. Eq. (42) can be regarded as a relation between the sum of dimer splittings and the quasiresonance shift of the monomer energy. For example, in the case of naphthalene-h_8 in naphthalene-d_8, it is known[2f] that $E(1)=31\,542$ cm^{-1}, $dE(1)/d\Delta$ can be estimated to be approximately 0.7, and $\Delta=-115$ cm^{-1}. For the host (naphthalene-d_8) $\epsilon(\mathbf{k}^-=0)=31\,587$ cm^{-1} and $\epsilon(\mathbf{k}^+=0)=31\,751$ cm^{-1}. From these experimental values we get roughly

$$\sum_{R_\alpha} S_{R_\alpha} = -43 \text{ cm}^{-1}$$

and

$$\sum_{R_\beta} S_{R_\beta} = 80 \text{ cm}^{-1}.$$

Experimentally, Hanson's data[4] give, respectively, -25.3 cm^{-1} and 61.2 cm^{-1}. Since the assumption of dimer splittings being small compared to the trap depth is not completely justified in this case, a discrepancy is expected. Furthermore the experimental values do not include more distant, and hence smaller, pair interactions.

D. Pairwise Interactions and Octupole Model

In the past, many attempts have been made by various authors[32] to discuss the intermolecular exciton interactions in the spirit of the point multipole expansion. These efforts were probably inspired by the prospect of being able to express the exciton interactions in terms of a relatively small number of multipole parameters which can, hopefully, be transferred from system to system (like from $C_{10}H_8$ in $C_{10}D_8$ to $C_{10}H_8$ in durene). The obvious drawback is the poor convergence of such an expansion as it is used in solids where molecules are in proximity. Craig and Walmsley[9] used this technique for $^1B_{2u}$ naphthalene by fitting the octupole parameters with the Davydov splitting (and the polarization ratio). Since the Davydov splitting is mostly accounted for by the interaction M_{12} between the nearest interchange-equivalent molecules, this raises a serious question about convergence. It is believed here that, if the octopole model is to work, we have a better chance of fitting the octopole parameters with the interactions between more distant, translationally equivalent, molecules. In doing this we are, of course, sacrificing the experimental accuracy associated with the measurement of larger interaction terms for a theoretically more justified expansion, i.e., one with a better convergence.

The octopole–octopole interactions for translationally equivalent pairs can be conveniently derived from the procedures discussed by Buckingham.[33a] In order to check any possible electron overlap, we have projected the molecules from the crystallographic coordinates to the molecular Cartesian coordinates. Figure 14 shows such a projection. The translationally equivalent molecules are either well staggered or have a large plane-to-plane distance. We included in our calculations all the lower order multipole parameters: Q_1^{1c}, Q_3^{1c}, and Q_3^{3c}. The (transition dipole) Q_1^{1c} is known[9] to be about 0.03 Å. The whole possible ranges of Q_3^{1c} and Q_3^{3c}, as suggested by Craig and Walmsley,[9] have been covered (including also all the possible relative signs between Q_1^{1c}, Q_3^{1c}, and Q_3^{3c}). For each set of octopole parameters, the rms of the deviations between the calculated and the experimental M_a, M_b, M_c, and M_{a+c} was tabulated and compared. The Franck–Condon factor for the 0–0 transition of $^1B_{2u}$ naphthalene was explicitly included. The experimental sets of M_a, M_b, M_c, and M_{a+c} consist of *all* the 24 sets (six sets from Tables I and II and all the possible permutations involving the exchanges $M_a \leftrightarrow M_b$ and $M_c \leftrightarrow M_{a+c}$). It is somewhat unexpected that there is only *one* set of interactions (M's) which can be meaningfully fitted with such a model. As tabulated in Table IV, one possible choice from set 1 can be nicely generated with multipole parameters of $Q_1^{1c}=0.03$ Å, $Q_3^{1c}=7$ Å^3, and $Q_3^{3c}=72$ Å^3.

It is not clear whether the above nice fit has any significance.[33b] The same parameters obviously will not

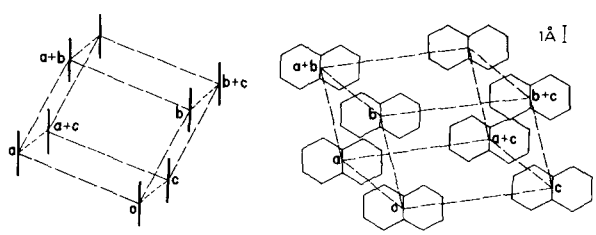

FIG. 14. Projections of naphthalene molecules in one sublattice of a naphthalene crystal onto the molecular plane (right-hand side) and the plane perpendicular to it and containing the short molecular axis (left-hand side). The unit cell is indicated by the dashed lines. Carbon skeletons are drawn to scale.

fit the Davydov splitting (which has been fitted by Craig and Walmsley with $Q_3^{1c}=9$ Å^3, $Q_3^{3c}=-12$ Å^3). On the other hand, it can always be argued that for the short-range, nearest-neighbor interaction (M_{12}), which is the major contribution to the Davydov splitting, the validity of the truncated point multipole expansion is rather questionable. We have attempted to transfer these parameters to the naphthalene-in-durene system. Some preliminary dimer data[34] obtained in this laboratory do not compare favorably with the theoretical values. However, the experimental values are by no means final, the site field differs and, besides, here we also encounter the problem of molecules in proximity (the **b** dimer being only 5.77 Å apart).

E. Experimental and *Ab Initio* Methods

Before any comparison between our "experimental" results and those of "*ab initio*" calculations is made, a word of caution is necessary. Our "first-order" exciton formalism for pure crystals is based on zeroth-order "site" functions while the only computations available were done with zeroth-order approximate molecular functions. One should therefore only compare final results. Furthermore, our numerical results are for the 0–0 vibronic exciton band, not for the entire electronic band, and for intercomparison one has to use a Franck–Condon factor of about 160/195.

Greer *et al.*[3c] claim that their configuration interaction ("charge transfer") terms do contribute most of the experimental site shift. However, the roles of the Franck–Condon factors in modifying the "effective" site shift were not at all clear in their paper. On the one hand, an "effective" Franck–Condon factor of 0.6 was introduced for benzene to get agreement with experiments while, on the other hand, it was implicitly assumed to be unity for naphthalene. The important point to note here is that if such a factor were formally introduced for naphthalene, it would have affected the contribution of the charge transfer states to the Davydov splitting and, consequently, reduced the magnitude of the adjustable octopole parameters.

TABLE IV. The pairwise interactions as fitted with the multipole parameters: $Q_1^{1c}=0.03$ Å, $Q_3^{1c}=7$ Å^3, $Q_3^{3c}=72$ Å^3.

	Pairwise interaction			
	M_a	M_b	M_c	M_{a+c}
Set 1[a]	−0.6	−3.9	−3.7	6.1
Over-all electronic interactions[b]	−0.73	−4.8	−4.5	7.4
Octopole model	−0.37	−4.6	−3.9	7.8
Deviation[c]		0.80		

[a] Taken from Table I, notice the permutation of M_a and M_{a+c}.
[b] Corrected for the Franck–Condon factor of 160/195 for the 0–0 transition.
[c] Sum of the squares of the differences between the second and the third rows.

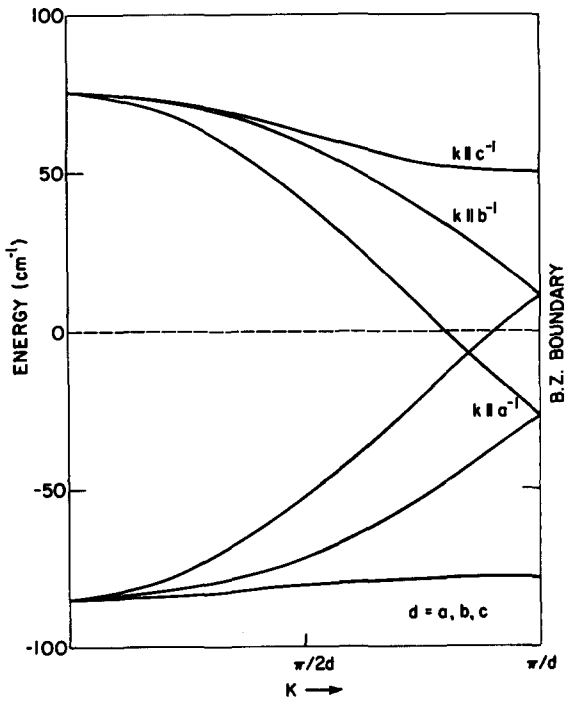

FIG. 15. The energy dispersion for the 0–0 exciton band of naphthalene $^1B_{2u}$ state along the three Brillouin zone axes. The band center is at the origin. The parameters used here are taken from Table IV.

The differences between the octopole parameters of Greer *et al.* and those of Craig and Walmsley[9] are quite insignificant. These parameters would, in both cases, be considered as too large compared with computed free molecule values. In our approach, we deal with "renormalized" molecular *site* functions which include, by definition, some of the higher-order configuration interaction contributions of the *molecular* function approach. These site states could, in principle, have octopole moments that are considerably different from the molecular values. It should be emphasized that a small site shift does not preclude a much larger moment distortion due to the same site (environmental) effect. In addition, we do not trust the accuracy of presently available π-electron-only naphthalene wavefunctions, especially when it comes to the calculation of properties that depend crucially on the details of the "tail end" of these functions. Such properties would include intermolecular interactions in general and higher-order transition moments in particular. One final point is that the octopole moments of Greer *et al.* are not really *ab initio* values. Similarly to those obtained by Craig and Walmsley, these moments were derived by fitting the experimental Davydov splitting. As we have mentioned earlier, this procedure essentially involves the fitting of multipole expansion parameters to the nearest neighbor pairwise interaction. This probably results in poor convergence, due to charge overlap.

In order to facilitate a comparison between our

results and those of Greer *et al.* we have calculated (Fig. 15) some dispersion curves (for the same special **k** values given by Greer) using our dispersion relation [Eq. (43)] with our set of pairwise interactions from Table IV. Our curves differ significantly from those in Greer's Fig. 3, although the latter have been fitted to match the Davydov splitting (**k**=0). As the Davydov splitting is only determined by interchange equivalent interactions, it is not surprising that the largest discrepancies between the curves occur at the boundary of the Brillouin zone, where the translational equivalent interaction terms are dominant. It should also be noted that our translational shift is -4.5 ± 4 cm^{-1}, compared with an "experimental" value[35] of $+10$ cm^{-1} given by Greer *et al.*

In our opinion, future *ab initio* calculations should be aimed at the direct evaluation of pair interactions, which can be directly subjected to experimental investigations as we have demonstrated here. Our "experimental" deep-trap values should provide a challenging and meaningful criterion for evaluating the qualities of wavefunctions used in *ab initio* calculations. Until such high-quality wavefunctions are available, one may aim at improving and increasing the list of empirically known intermolecular pairwise interactions, with emphasis on both the radial and the angular dependence.

IV. SUMMARY

The purpose of this paper can be summarized as follows: (a) In the broader aspect, we have demonstrated how the multiple-scattering formalism developed previously for the multiple-branched exciton band behaves at the low concentration limit. The detailed structure of the average Green's function was further analyzed and its physical meaning was further exposed. (b) The resonance pair problem was treated within the framework of the "restricted Frenkel theory." The energy eigenstates and the optical properties were discussed together with some symmetry properties pertaining to the pairs. (c) Specifically, energy states of naphthalene-h_8 resonance pairs in naphthalene-d_8 were calculated with a six-parameter model. It was shown that quasiresonance interactions cannot be neglected. This leads to the introduction of the concept of exciton superexchange which, in this case, largely overwhelms the direct excitation exchange for some translationally equivalent pairs. It was also demonstrated how this superexchange effect can be utilized in assigning the resonance pair spectra. (d) Six sets of intermolecular interaction parameters were obtained. It was found that three of these also give a density-of-states function consistent with the hot-band data and the monomer energies derived experimentally. Therefore, all the experimental data presently available can be explained by these parameters. (e) It was also concluded that phonons have little effect on the "experimental density-of-states function". The latter represents, to a large extent, the "true" exciton band profile. (f) The octopole model was also tested, not by fitting the Davydov splitting but by fitting the pairwise interactions with the exclusion of nearest neighbors. A unique fit gives octopole parameters of $Q_3^{1c}=7$ Å^3 and $Q_3^{3c}=72$ Å^3. However, it was emphasized that this might be a fortuitous result. (g) A method for determining the complete exciton band structure is now available for the "restricted Frenkel–Davydov" case and has been demonstrated for the first excited singlet state of naphthalene.

* Supported by the National Institute of Neurological Diseases and Stroke, Grant No. RO1 NS08116.

[1] (a) J. Frenkel, Phys. Rev. **37,** 1276 (1931); (b) A. S. Davydov, *Theory of Molecular Excitons* (McGraw-Hill, New York, 1962); (c) A. S. Davydov Usp. Fiz. Nauk **82,** 393 (1964) [Sov. Phys. Usp. **7,** 145 (1964)].

[2] (a) M. A. El-Sayed, M. T. Wauk, and G. W. Robinson, Mol. Phys. **5,** 205 (1962); (b) G. C. Nieman and G. W. Robinson, J. Chem. Phys. **39,** 1298 (1963); (c) S. D. Colson, R. Kopelman, and G. W. Robinson, *ibid.* **47,** 27 (1967); (d) S. D. Colson, D. M. Hanson, R. Kopelman, and G. W. Robinson, *ibid.* **48,** 2215 (1968); (e) E. R. Bernstein, S. D. Colson, R. Kopelman, and G. W. Robinson, J. Chem. Phys. **48,** 5596 (1968); (f) D. M. Hanson, R. Kopelman, and G. W. Robinson, *ibid.* **51,** 212 (1969).

[3] (a) R. Silbey, J. Jortner, M. T. Vala, and S. A. Rice, J. Chem. Phys. **42,** 2948 (1965); (b) R. Silbey, J. Jortner, and S. A. Rice, *ibid.* **43,** 3336 (1965); (c) W. L. Greer, S. A. Rice, J. Jortner, and R. Silbey, *ibid.* **48,** 5667 (1968).

[4] (a) D. M. Hanson, J. Chem. Phys. **52,** 3409 (1970); (b) D. M. Hanson, R. Kopelman, and G. W. Robinson, 21st Symposium on Molecular Structure and Spectroscopy, Ohio State University, Columbus, Ohio, September, 1966.

[5] (a) H. K. Hong, Ph.D. thesis, California Institute of Technology 1970; (b) H. K. Hong and G. W. Robinson, J. Chem. Phys. **54,** 1369 (1971).

[6] H. K. Hong and G. W. Robinson, J. Chem. Phys. **52,** 825 (1970).

[7] (a) F. Yonezawa and T. Matsubara, Progr. Theoret. Phys. (Kyoto) **35,** 357 (1966); (b) **35,** 759 (1966); (c) **37,** 1346 (1967).

[8] (a) G. F. Koster and J. C. Slater, Phys. Rev. **95,** 1167 (1954); **96,** 1208 (1954); (b) G. F. Koster, *ibid.* **95,** 1436 (1954).

[9] D. P. Craig and S. H. Walmsley, Mol. Phys. **4,** 113 (1961).

[10] (a) D. P. Craig and M. R. Philpott, Proc. Roy. Soc. (London) **A290,** 583, 602 (1966); and **A293,** 213 (1966). (b) B. S. Sommer and J. Jortner, J. Chem. Phys. **51,** 5559 (1969).

[11] Notice that we have implicitly used here the time reversal symmetry appropriate for nonmagnetic interactions, i.e., the pure crystal energies associated with the positive and negative reduced wave vector **k** are degenerate. See L. P. Bouckaert, R. Smoluchowski, and E. Wigner, Phys. Rev. **50,** 58 (1936). This relation guarantees that ρ_R is real.

[12] For consistency, the notation used here is kept the same as that of Ref. 6, unless mentioned otherwise.

[13] (a) The translationally equivalent and interchange equivalent pairs are named as such not because they actually possess translational or interchange symmetry *in the mixed crystal.* Rather, the impurities occupy two positions which are related by translational or interchange symmetry operations *in the pure crystal.* See discussions in Sec. II.B. (b) R. Kopelman, J. Chem. Phys. **47,** 2631 (1967).

[14] See, for example, R. D. Mattuck, *A Guide to Feynman Diagrams in Many-Body Problems* (McGraw-Hill, New York, 1967).

[15] (a) See Eqs. (39), (40), and (42b) of Ref. 6. Note that Σ in Eq. (4b) here is equivalent to Σ^* in Ref. 6. (b) Notice that the diagrammatic expansion of $\langle G(\mathbf{k}) \rangle$ in Fig. 1. is equivalent to that of Fig. 3 of Ref. 6.

[16] Some of the polynomials $P_\nu(c)$ with small ν are given in Ref. 6 and also Ref. 7(a). They are the same for single- and multiple-branched exciton bands.

[17] Notice that Eq. (6) here is equivalent to Eq. (28) of Ref. 6. We have a new symbol δ here instead of just δ, for clarity.

[18] S. F. Edwards, Phil. Mag. **3,** 1020 (1958).

[19] R. Klauder, Ann. Phys. (N.Y.) **14,** 43 (1961).

[20] The dual symmetry has been discussed in Refs. 7 and 6. See also Y. Onodera and Y. Toyozawa, J. Phys. Soc. Japan **24,** 341 (1968).

[21] Only bound states outside the host band are considered here. For states inside the band, the approximation used here will no longer be valid. For more complete discussions on states inside the band, see A. Shibatani and Y. Toyozawa, J. Phys. Soc. Japan **25,** 335 (1968).

[22] E. I. Rashba, Opt. Spektrosk. **2,** 568 (1957).

[23] (a) R. G. Body and I. G. Ross, Australian J. Chem. **19,** 1 (1966); (b) B. S. Sommer and J. Jortner J. Chem. Phys. **50,** 187, 822, (1969).

[24] I. M. Lifschitz, Advan. Phys. **13,** 483 (1964).

[25] (a) In general, the crystal symmetry of naphthalene is such that any interactions between molecules in the **ac** plane can be included in the dispersion relation without invalidating the restricted Frenkel–Davydov limit. See R. Kopelman and J. C. Laufer, in "Electronic Density of States", edited by L. H. Bennett, National Bureau of Standards Spec. Publ. **323** (to be published). (b) It is easy to show that both the density-of-states function and the dimer energies will not be changed with the interchange of M_c and M_{a+c}. To illustrate this, we simply make the following transformation for Eq. (43):

$$\mathbf{a}\rightarrow-\mathbf{a}',\ \mathbf{a}+\mathbf{c}\rightarrow\mathbf{c}',\quad\text{and}\quad\mathbf{c}\rightarrow\mathbf{a}'+\mathbf{c}'.$$

It can be shown that Eq. (43) now becomes:

$$\begin{aligned}\epsilon'(\mathbf{k}^{\pm})=&\,2M_a\cos(\mathbf{k}\cdot\mathbf{a}')+2M_b\cos(\mathbf{k}\cdot\mathbf{b})\\&+2M_c\cos[\mathbf{k}\cdot(\mathbf{a}'+\mathbf{c}')]+2M_{a+c}\cos(\mathbf{k}\cdot\mathbf{c}')\\&\pm\{4M_{12}\cos[\mathbf{k}\cdot(\mathbf{a}'/2)]\cos[\mathbf{k}\cdot(\mathbf{b}/2)]+4M_{12}'[\cos(\mathbf{k}\cdot\mathbf{c}')\\&\times\cos(\mathbf{k}\cdot\mathbf{a}'/2)\cos(\mathbf{k}\cdot\mathbf{b}/2)-\sin(\mathbf{k}\cdot\mathbf{c}')\sin(\mathbf{k}\cdot\mathbf{a}'/2)\cos(\mathbf{k}\cdot\mathbf{b}/2)]\}.\end{aligned}\tag{43'}$$

Apparently, if we make the interchange $M_c\rightarrow M_{a'+c'}$, $M_{a+c}\rightarrow M_{c'}$ there is a one-to-one correspondence between $\epsilon'(\mathbf{k}^{\pm})$ and $\epsilon'(\mathbf{k}^{\pm})$. Therefore the density-of-states function will stay the same. It is also obvious that the $\mathbf{c}'$ and $(\mathbf{a}'+\mathbf{c}')$ dimers have exactly the same energies, respectively, as the $(\mathbf{a}+\mathbf{c})$ and $\mathbf{c}$ dimers. Because of the topological structure we will not be able to distinguish between the two dimers, with our present six-parameter model. On the other hand, the interchangability of M_a and M_b is essentially empirical and not rigorous. As we can see from Table I and II, the "superexchange" terms for **a** and **b** dimers are quite similar. It is also found that the density-of-states function is practically unchanged when M_a and M_b are interchanged. The only theoretical justification for the above is that M_{12} is large. For the case of "superexchange," we can see from the second moments in Sec. III.B that $m_a^{(2)}=m_b^{(2)}$ if M_{12} is large. Using the same moment method we can show that also the density-of-states function is only slightly altered with respect to the same interchange.

[26] P. W. Anderson, *Solid State Physics*, edited by F. Seitz and D. Turnbull (Academic, New York 1963), Vol. **14,** pp. 99–214.

[27] Further utilization can be made by using three-component systems. Such observations already exist although quite unintentionally. The "hyperfine" doublets observed by Hanson[4a] on three "monomer" lines (his Table IV) and on at least one "dimer" component (his Table II) can now be explained as due to the presence of about 10%–15% mole $C_{10}HD_7$ (α and β combined) in the $C_{10}D_8$ host. Preliminary calculations show that the hyperfine energy splitting and the relative intensities are consistent with an appropriate generalization of the quasiresonance and superexchange concepts. Calculations and experiments on this and other systems are underway.

[28] R. Kopelman, J. Chem. Phys. **44,** 3547 (1966).

[29] Y. A. Izyumov, Advan. Phys. **14,** 569 (1965).

[30] Due to the large perturbations on the vibrational quanta by isotopic substitutions, it is simple to select a convenient vibronic band with large trap depth. The actual difficulty will probably be the selection of a band with appreciable Davydov splitting. In the event that such a vibronic band can be studied, pairwise interactions can always be related to those of the 0–0 band by proper adjustments with Franck–Condon factors.

[31] (a) Notice that we have discarded part of the density-of-states function above the *ac* Davydov component (compare Figs. 10, 11). Renormalization was not done because the change is relatively insignificant. (b) It is reasonable and consistent to assume that phonon complications on the neat crystal dispersion relation are of the same order as for the density of states. Hence we believe that the dispersion relation given in Eq. (43), with the parameter values from Table I (see also Fig. 15), actually applies to the pure crystal, even though it has been derived from resonance pairs. Incidentally, the above discussion assumes negligible phonon effects on the resonance pair splittings. This is very reasonable to assume, as the pairwise exciton interactions (less than 20 cm^{-1}) are all smaller than the *impurity localized phonon frequencies* [D. M. Hanson, J. Chem. Phys. **51,** 5063 (1969)], which should be very similar for isolated guests and for guest pairs. Essentially one deals here with an analogy of the Simpson and Petersen weak coupling case (phonons replacing internal vibrations). In view of the additional fact that the zero-phonon line is the most intense by far in impurity spectra of naphthalene-h_8 in naphthalene-d_8, we conclude that most of the Franck–Condon overlap (again replacing internal vibrations by phonons) is in the zero-phonon line. This means that no exciton splitting is "borrowed" by the phonon addition levels of the resonance pairs (the appropriate spectroscopic transitions are too weak to be observed). Finally we still stress the fact that our exciton interactions are derived from a *real lattice*, including zero-point vibrations.

[32] D. Fox and O. Schnepp, J. Chem. Phys. **23,** 767 (1955). See also Refs. 1(b), 1(c), 3, and 9.

[33] (a) A. D. Buckingham, Quart. Rev. Chem. Soc. London **13,** 183 (1959). (b) We have used the same multipole parameters to calculate interactions of further removed pairs. All such M's are less than 2 cm^{-1}. This is consistent with both the experimental splittings[4] and with the restricted Frenkel-Davydov model. See also Footnote 25(a).

[34] P. H. Chereson and R. Kopelman, 24th Symposium on Molecular Structure and Spectroscopy, Ohio State University, Columbus, Ohio, 1969.

[35] Incidentally, the derivation by Greer *et al.*[3b] of this *translational shift* is equivalent to the following operation: captain+ship−(similar ship)=captain (?!). Furthermore, if the translational shift were +10 cm^{-1}, the band center of naphthalene-h_8 would be at 31 544 cm^{-1}. Since the monomer energy of naphthalene-h_8 in naphthalene-d_8 is at 31 542 cm^{-1} according to Greer *et al.*, the quasiresonance shift would be only 2 cm^{-1}, which seems to be unreasonably small.